CHEMISTRY OF MATERIALS

ARTICLE

pubs.acs.org/cm

Design of New Electron Acceptor Materials for Organic Photovoltaics: Synthesis, Electron Transport, Photophysics, and Photovoltaic Properties of Oligothiophene-Functionalized Naphthalene Diimides

Eilaf Ahmed, Guoqiang Ren, Felix S. Kim, Emily C. Hollenbeck, and Samson A. Jenekhe*

Department of Chemical Engineering and Department of Chemistry, University of Washington, Seattle, Washington 98195-1750, United States

Supporting Information

ABSTRACT: A homologous series of six novel oligothiophene–naphthalene diimide-based oligomer semiconductors with a donor–acceptor architecture, NDI-*n*TH (n = 1, 2, 3, 4) and NDI-*n*T (n = 2, 3), was synthesized and used to explore a set of criteria for the design of *non-fullerene* electron acceptor materials for organic solar cells. Thin films of the oligomer semiconductors had optical band gaps that varied from 2.1 eV in NDI-1TH and 1.6 eV in NDI-3TH to 1.4 eV in NDI-4TH, demonstrating good potential for light harvesting and exciton generation. The LUMO energy levels of the oligomer semiconductors were similar (ca. −4.0 eV), but the HOMO levels varied from −5.5 eV in NDI-3TH and NDI-4TH to −6.1 eV in NDI-1TH, showing that suitable energy band offsets necessary for efficient photoinduced charge transfer could be achieved with current donor polymers. Single-crystal X-ray structures of NDI-3TH and NDI-4TH showed a slipped face-to-face π-stacking with short intermolecular distances (0.321–0.326 nm), which enabled facile self-assembly of single-crystalline nanowires from solution. Spin coated thin films of NDI-*n*TH and NDI-*n*T were mostly crystalline and had field-effect electron mobilities of up to $(2–9) \times 10^{-4}$ cm^2/(V s). Bulk heterojunction solar cells incorporating one of the n-type oligomer semiconductors as the electron acceptor and poly(3-hexylthiophene) as the electron donor showed a power conversion efficiency of 1.5% with an open circuit voltage of 0.82 V and a bicontinuous nanoscale morphology.

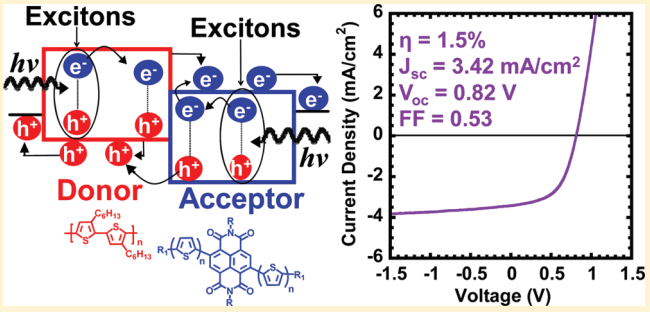

KEYWORDS: organic solar cell, photovoltaic, organic field-effect transistor, n-type organic semiconductor, naphthalene diimide, donor–acceptor oligomer, *non-fullerene* electron acceptor, charge transport

1. INTRODUCTION

Organic photovoltaics (OPVs) are promising for developing low cost solar energy conversion technologies.[1−10] Because light absorption in OPVs initially generates strongly bound excitons,[2] an electron donor–acceptor interface with suitable HOMO/LUMO energy level offsets is necessary for efficient charge photogeneration.[1,3] Among the different OPV device architectures explored to date, including the Schotky barrier[4] and bilayer heterojunction[5] cells, the bulk heterojunction (BHJ) cell[6] with an active layer consisting of a blend of a donor polymer and an acceptor material provides the most efficient example of these excitonic solar cells.[7−10] Although other acceptor materials such as inorganic nanocrystals (CdSe,[11] PbS,[12] TiO_2,[13] etc), carbon nanotubes,[14] graphene sheets,[15] n-type conjugated small molecules,[16−21] and n-type polymer semiconductors[6,22−26] have been explored, fullerene-based acceptors have demonstrated excellent electron-accepting[27] and electron-transport[28] properties and have thus dominated the field of OPVs.[1−10] Indeed, much progress has been made in polymer/fullerene BHJ solar cells, including substantial improvements in the power conversion efficiency to current maximum levels of 6–8%[7] as well as understanding of the critical role of the BHJ nanoscale morphology[9,29−32] and the origin of the open circuit voltage (V_{oc}).[33] However, fullerene acceptors have important drawbacks in OPVs: (i) they have negligible light absorption in the visible-near IR region;[1,34] (ii) they have relatively poor photochemical and chemical stability,[35] requiring extensive encapsulation for the operation of the OPVs in air; (iii) their much higher rates of molecular diffusion and crystallization compared to those of the donor polymer component pose challenges for the control of the phase-separation kinetics and the BHJ film morphology;[1b,e] (iv) their accessible LUMO energy levels are in a very narrow range, limiting the accessible photovoltage; (v) the available chemistry for the synthesis of fullerene derivatives is limited;[36] and (vi) the cost of fullerene synthesis and purification is high.[22] There is thus a major need to investigate and discover new n-type organic semiconductors that could potentially replace fullerene acceptors in OPVs.

Small-molecule organic semiconductors[16−21] and various conjugated polymers[6,22−26] have been explored as *non-fullerene* acceptor materials in OPVs of bilayer heterojunction and bulk

Received: July 10, 2011
Revised: September 5, 2011
Published: September 30, 2011

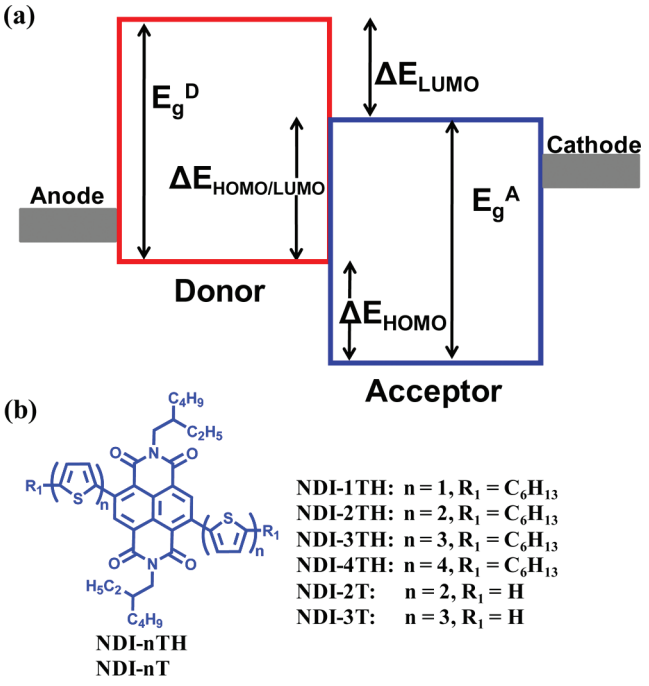

Figure 1. (a) Schematic of a typical donor/acceptor interface in a BHJ solar cell with associated HOMO/LUMO energy level offsets. (b) Molecular structures of oligothiophene-functionalized NDIs.

heterojunction (BHJ) architectures. Among these n-type organic semiconductors that have been studied in *non-fullerene* OPVs are cyano-poly(phenylenevinylene) (CN-PPV),[6b,24] poly(benzobisimidazobenzophenanthroline) (BBL),[23] polyfluorene(benzothiadiazole)) (F8TBT),[26] perylene diimides,[18,19,25] vinazene derivatives,[20] cyanopentacenes,[16,21] bifluorenylidene,[17a] and diketopyrrolopyrrole derivatives.[17b,c] The highest power conversion efficiency of BHJ solar cells using these n-type small molecules varies from 1.87% PCE in perylene diimides derivatives,[19d] 1.29% PCE in cyanopentacene,[21b] and 1.4% PCE in vinazene derivatives[20c] to 1% PCE in diketyopyrrolopyrrole derivatives.[17b,c] Among the major current challenges in developing more efficient *non-fullerene* BHJ polymer solar cells is the lack of suitable n-type organic semiconductors that combine solution processability with suitable HOMO/LUMO energy levels, good charge transport, and other properties. Indeed, the factors essential to the design and development of new electron acceptor materials for the realization of more efficient *non-fullerene* OPVs remain to be elucidated.

In this paper, we explore the design of new, *non-fullerene*, n-type organic semiconductors for use as efficient electron acceptors and electron-conducting materials in OPVs. Toward this end, we identify the following major considerations and design criteria: (1) The HOMO/LUMO energy levels of the acceptor material relative to those of the donor polymer semiconductor should offer sufficient offsets to facilitate photoinduced electron/charge transfer and efficient charge separation while maximizing the photovoltage (Figure 1a). A common LUMO/LUMO offset (ΔE_{LUMO}) thought to be necessary in the case of a donor polymer and a fullerene acceptor is 0.12−0.3 eV;[1,37] this value is still a relevant guide in the case of new *non-fullerene* acceptors. Although the HOMO/HOMO offset (ΔE_{HOMO}) has not been an important consideration with fullerene acceptors and donor polymers because of the rather deep HOMO level of fullerene acceptors (HOMO = −6.0 eV),[38] a ΔE_{HOMO} at 0.2−0.3 eV or larger is necessary to inject holes and confine them to the donor polymer. As is already well-known, the maximum possible open circuit voltage (V_{oc}) is directly related to the HOMO/LUMO offset ($\Delta E_{HOMO/LUMO}$) of the active donor and acceptor in the OPV.[1,3,33] (2) To facilitate good charge transport and efficient charge collection at the electrodes, the acceptor material should have a high electron mobility ($\mu_e > 10^{-4}$–10^{-3} $cm^2/(V\ s)$). (3) The absorption band and optical band gap (E_g^A) of the acceptor material should contribute to light harvesting and exciton generation, and ideally, they should be complementary[23] to those of the donor polymer (E_g^D) in the visible-near IR spectral range. (4) To facilitate favorable acceptor material/donor polymer blend phase separation thermodynamics and kinetics in forming the BHJ active layer film, the acceptor material should have a sufficiently large molar mass. (5) The solubility of the acceptor material in common organic solvents is essential to realize solution-based processing and the fabrication of OPVs. (6) The purity of the acceptor material should be sufficiently high (electronic grade) to enable high performance OPVs.

To evaluate the criteria for the design of new acceptor materials for OPVs, we targeted a homologous series of π-conjugated oligomers with a donor−acceptor (D−A) architecture containing a central naphthalene diimide (NDI) electron-withdrawing group and appended electron-donating oligothiophenes of varying size (Figure 1b). We selected to focus on oligomers because they have a discrete molecular size, which should enable reproducible synthesis and ready tunability of HOMO/LUMO energy levels and other properties necessary to realize many of the design criteria. The D−A architecture of the oligothiophene-functionalized NDI molecules (NDI-*n*TH, *n* = 1, 2, 3, 4; NDI-*n*T, *n* = 2, 3) by virtue of intramolecular charge transfer (ICT) interactions[39a] can provide a facile means of tuning the optical band gaps, HOMO/LUMO energy levels, and charge carrier mobilities.[39b,c] NDI-based small molecules (evaporated thin films) and polymers (spin coated thin films) are known to exhibit n-channel organic field-effect transistor properties with high carrier mobilities.[40−44] In this paper, we report the synthesis, crystal structures, photophysics, electrochemical redox properties, and charge transport properties of the novel oligothiophene-functionalized naphthalene diimides shown in Figure 1b. The initial use of the materials as acceptors in bulk heterojunction solar cells in combination with a model donor polymer, poly(3-hexylthiophene) (P3HT), is also reported. The results are discussed in the context of the identified criteria for the design of acceptor materials toward more efficient *non-fullerene* OPVs.

2. EXPERIMENTAL SECTION

2.1. Materials and Synthetic Procedures. Regioregular poly(3-hexylthiophene) (P3HT) was purchased from Rieke Metals with weight-average molecular weight (M_w) of 35.40 KDa and polydispersity index (PDI) of 2.45. All commercially obtained reagents were used without further purification.

N,N′-Bis(2-ethylhexyl)-2,6-bis(5-hexyl-thiophen-2-yl)-1,4,5,8-naphthalene Diimide (NDI-1TH). 2,6-Dibromonaphthalene diimide (**1**) (350 mg, 0.540 mmol), 5-hexyl-2-trimethylstannylthiophene (**2a**) (540 mg, 1.63 mmol), and palladium-tetrakis(triphenylphosphine) Pd-$(PPh_3)_4$ (31 mg, 0.0268 mmol) were added to a flask under argon. The flask was degassed with argon three times, followed by the addition of 15 mL of anhydrous toluene, and the mixture was refluxed overnight. The product was purified by column flash chromatography using a

dx.doi.org/10.1021/cm2019668 |*Chem. Mater.* 2011, 23, 4563–4577

dichloromethane and hexane solvent mixture. The pure product was recrystallized from the dichloromethane/methanol mixture to give a red solid (212 mg, 48% yield). HRMS (FAB) (m/z) calcd for $C_{50}H_{66}N_2O_4S_2$ [$(M + H)^+$] 823.4464, found 823.45709. ^{1}H NMR (CD_2Cl_2, 300 MHz, ppm): δ 8.7680 (s, 2H), 7.203 (d, J = 3.6 Hz, 2H), 6.8812 (d, J = 3.5 Hz, 2H), 4.0801 (d, J = 5.9 Hz, 4H), 2.9351 (t, J = 7.7 Hz, 4H), 1.934 (m, 2H), 1.797−1.719 (m, 4H), 1.424−1.274 (m, 29H), 0.956−0.865 (m, 18H). ^{13}C NMR (CD_2Cl_2, 500 MHz, ppm): δ 162.554, 162.516, 146.647, 140.925, 139.135, 139.093, 136.245, 134.009, 129.793, 127.528, 125.430, 125.067, 124.073, 123.047, 122.806, 44.439, 37.855, 31.592, 31.577, 30.647, 30.164, 28.765, 28.613, 23.917, 23.123, 22.608, 13.886, 13.861, 10.348.

N,N′-Bis(2-ethylhexyl)-2,6-bis(5′-hexyl[2,2′]bithiophenyl-5-yl)-1,4,5,8-naphthalene Diimide (NDI-2TH). 2,6-Dibromonaphthalene diimide (**1**) (318 mg, 0.490 mmol), 5-hexyl-2-trimethylstannylbithiophene (**2b**) (890 mg, 2.15 mmol), and $Pd(PPh_3)_4$ (28 mg, 0.024 mmol) were added to a flask under argon. The flask was degassed with argon three times, followed by addition of 20 mL of anhydrous toluene, and the mixture was refluxed for 18 h. The product was purified by column flash chromatography using a dichloromethane and hexane mixture. The pure product was collected and redissolved in chloroform and precipitated from methanol. The pure product was obtained as a dark blue solid (384 mg, 79% yield). HRMS (FAB) (m/z) calcd for $C_{58}H_{70}N_2O_4S_4$ [$(M + H)^+$] 987.43015, found 987.43403. ^{1}H NMR (CD_2Cl_2, 300 MHz, ppm): δ 8.779 (s, 2H), 7.307 (d, J = 3.8 Hz, 2H), 7.230 (d, J = 3.8 Hz, 2H), 7.139 (d, J = 3.6 Hz, 2H), 6.798 (d, J = 3.6 Hz, 2H), 4.125 (d, J = 7.6 Hz, 4H), 2.872 (t, J = 7.4 Hz, 4H), 1.940 (m, 2H), 1.771−1.721 (m, 4H), 1.475−1.297 (m, 29H), 0.980−0.894 (m, 18H). ^{13}C NMR (CD_2Cl_2, 500 MHz, ppm): δ 162.554, 162.516, 146.647, 140.925, 139.135, 139.093, 136.245, 134.009, 129.793, 127.528, 125.430, 125.067, 124.073, 123.047, 122.806, 44.439, 37.855, 31.592, 31.577, 30.647, 30.164, 28.765, 28.613, 23.917, 23.123, 22.608, 13.886, 13.861, 10.348.

*Compound **5***. 2,6-Dibromonaphthalene diimide (**1**) (627 mg, 0.967 mmol), 2-tributylstannylthiophene (1.08 g, 2.89 mmol), $Pd(PPh_3)_4$ (56 mg, 0.048 mmol), and 20 mL of anhydrous toluene were added to a flask under argon. The mixture was refluxed for 18 h. The crude product was purified by column flash chromatography using a dichloromethane and hexane mixture (3:2). The pure product was obtained as a red solid (546 mg, 86% yield). LC-MS (m/z) [$(M + H)^+$] found 655.4, required 654.88. ^{1}H NMR ($CDCl_3$, 300 MHz, ppm): δ 8.768 (s, 2H), 7.203 (d, J = 3.6 Hz, 2H), 6.881 (d, J = 3.5 Hz, 2H), 4.118 (d, J = 7 Hz, 4H), 2.921 (t, J = 7.7 Hz, 4H), 1.932 (m, 2H), 1.475−1.268 (m, 16H), 0.891 (m, 12H).

N,N′-Bis(2-ethylhexyl)-2,6-bis([2,2′]bithiophenyl-5-yl)-1,4,5,8-naphthalene Diimide (NDI-2T). 2,6-Dibromonaphthalene diimide (**1**) (560 mg, 0.87 mmol), 2-tributylstannylthiophene (**4**) (1.19 g, 2.61 mmol), $Pd(PPh_3)_4$ (50 mg, 0.043 mmol), and 20 mL of anhydrous toluene were added to a flask under argon. The mixture was refluxed for 18 h. The product was purified by column flash chromatography using a chloroform/hexane solvent mixture (3:2). The purified product was collected and redissolved in chloroform and precipitated from methanol. The pure product was obtained as a blue solid (615 mg, 86% yield). HRMS (FAB) (m/z) calcd for [$(M + H)^+$] $C_{46}H_{47}N_2O_4S_4$ 819.24159, found 819.24212. ^{1}H NMR (CD_2Cl_2, 300 MHz, ppm): δ 8.795 (s, 2H), 7.375−7.316 (m, 8H), 7.128 (d, 2H), 4.131 (d, 4H), 1.942 (m, 2H), 1.4607−1.3066 (m, 20H), 0.9828−0.8838 (m, 12H). ^{13}C NMR (CD_2Cl_2, 500 MHz, ppm): δ 162.507, 162.488, 140.157, 139.815, 139.123, 136.714, 136.272, 129.671, 128.057, 127.568, 125.508, 125.248, 124.361, 123.866, 123.067, 44.466, 37.853, 30.634, 28.596, 23.915, 23.110, 13.869, 10.345.

*Compound **6***. Compound **5** (373 mg, 0.569 mmol) was dissolved in 15 mL of chloroform and 5 mL of DMF. In a different flask, NBS (240 mg, 1.35 mmol) was dissolved in 5 mL of chloroform and 10 mL of DMF and added slowly via an addition funnel to compound **5**. The reaction mixture was stirred in the dark for two days. The product was purified by column chromatography using a dichloromethane and hexane mixture. The pure product was collected as a red solid (443 mg, 96% yield). LC-MS (m/z) ($M - H^+$) found 812.2, requires 812.67. ^{1}H NMR ($CDCl_3$, 300 MHz, ppm): δ 8.739 (s, 2H), 7.174 (d, 2H), 7.109 (d, 2H), 4.114 (d, 4H), 1.919 (m, 2H), 1.398−1.294 (m, 16H), 0.956 (m, 12H).

*Compound **7***. NDI-2T (490 mg, 0.60 mmol) was dissolved in 17 mL of chloroform and 5 mL of DMF. NBS (220 mg, 1.23 mmol) was dissolved in 5 mL of chloroform and 10 mL of DMF and added slowly to NDI-2T. The reaction mixture was stirred in the dark for two days. The product was extracted with dichloromethane, washed with water and brine solution, and the organic solvent was evaporated. The blue solid was purified by column chromatography using a dichloromethane/hexane (5:1) solvent mixture to give the final product (496 mg, 85% yield). ^{1}H NMR (CD_2Cl_2, 300 MHz, ppm): δ 8.776 (s, 2H), 7.317 (dd, 4H), 7.091 (m, 4H), 4.114 (d, 4H), 1.932 (m, 2H), 1.457−1.320 (m, 18H), 0.977−0.777 (m, 12H).

N,N′-Bis(2-ethylhexyl)-2,6-bis(5″-hexyl[2,2′;5′,2″]terthiophen-5-yl)-1,4,5,8-naphthalene Diimide (NDI-3TH). Compound **6** (440 mg, 0.545 mmol), 5-hexyl-2-trimethylstannylbithiophene (**2b**) (670 mg, 1.62 mmol), and $Pd(PPh_3)_4$ (31 mg, 0.027 mmol) were added to a flask under argon. The flask was degassed with argon three times, followed by addition of 20 mL of anhydrous toluene, and the mixture was refluxed for 24 h. The product was purified by column flash chromatography using a chloroform and hexane mixture. The pure product was collected and redissolved in chloroform and precipitated from methanol. The pure product was obtained as a dark green solid (377 mg, 60% yield). HRMS (ESI) (m/z) calcd for $C_{66}H_{75}N_2O_4S_6$ 1151.4046, found 1151.4059. ^{1}H NMR (CD_2Cl_2, 300 MHz, ppm): δ 8.793 (s, 2H), 7.336 (dd, J = 3.8 Hz, 4H), 7.225 (d, J = 3.8 Hz, 2H), 7.114 (dd, J = 3.8 Hz, 4H), 6.776 (d, J = 3.6 Hz, 2H), 4.129 (d, J = 7.1 Hz, 4H), 2.854 (t, J = 7.6 Hz, 4H), 1.953−1.933 (m, 2H), 1.756−1.703 (m, 4H), 1.470−1.297 (m, 29H), 0.985−0.891 (m, 18H). ^{13}C NMR (CD_2Cl_2, 500 MHz, ppm): δ 162.546, 162.502, 146.238, 140.063, 139.744, 139.028, 137.683, 136.269, 134.721, 134.137, 129.893, 127.600, 125.493, 125.010, 124.995, 123.686, 123.670, 122.946, 44.479, 37.861, 31.603, 31.566, 30.643, 30.137, 28.751, 28.604, 23.919, 23.123, 22.595, 13.884, 13.848, 10.351.

N,N′-Bis(2-ethylhexyl)-2,6-bis(5″-hexyl-[2,2′;5′,2″;5″,2‴]quaterthiophen-5-yl)-1,4,5,8-naphthalene Diimide (NDI-4TH). Compound **7** (623 mg, 0.638 mmol), compound **2b** (681 mg, 1.66 mmol), and $Pd(PPh_3)_4$ (37 mg) were added to a flask under argon. The flask was degassed with argon three times, followed by addition of 18 mL of anhydrous toluene, and the mixture was refluxed for 12 h. The organic phase was washed with water and concentrated. The product was purified by column flash chromatography using a dichloromethane and hexane mixture. The product was collected and redissolved in chloroform and precipitated from methanol. The pure product was obtained as a dark green solid (265, 32% yield). MALDI-TOF MS (m/z) calcd 1314.3727, found 1313.844. ^{1}H NMR (CD_2Cl_2, 300 MHz, ppm): δ 8.792 (s, 2H), 7.322 (m, 4H), 7.237 (dd, 2H), 7.17 (t, 4H), 7.075 (m, 4H), 6.764 (m, 2H), 4.115 (dd, 4H), 2.846 (m, 4H), 1.749 (m, 4H), 1.469−1.333 (m, 18H), 0.989−0.893 (m, 12H). ^{13}C NMR ($CDCl_3$, 500 MHz, ppm): δ 162.570, 145.903, 140.494, 139.498, 139.266, 137.309, 137.045, 136.526, 135.392, 134.958, 134.335, 130.194, 127.586, 125.402, 125.154, 124.909, 124.515, 124.198, 123.952, 123.635, 123.564, 122.538, 44.673, 37.812, 31.591, 30.687, 30.236, 28.791, 28.623, 23.961, 23.149, 22.604, 14.150, 14.112, 10.645.

N,N′-Bis(2-ethylhexyl)-2,6-bis([2,2′;5′,2″]terthiophen-5-yl)-1,4,5,8-naphthalene Diimide (NDI-3T). Compound **7** (496 mg, 0.508 mmol), compound **3** (564 mg, 1.51 mmol), and $Pd(PPh_3)_4$ (29 mg) were added to a flask under argon. The flask was degassed with argon three times, followed by addition of 24 mL of anhydrous toluene, and the mixture was refluxed for 12 h. The organic phase was washed with water and

Scheme 1. Synthesis of Oligothiophene-Functionalized Naphthalene Diimides[a]

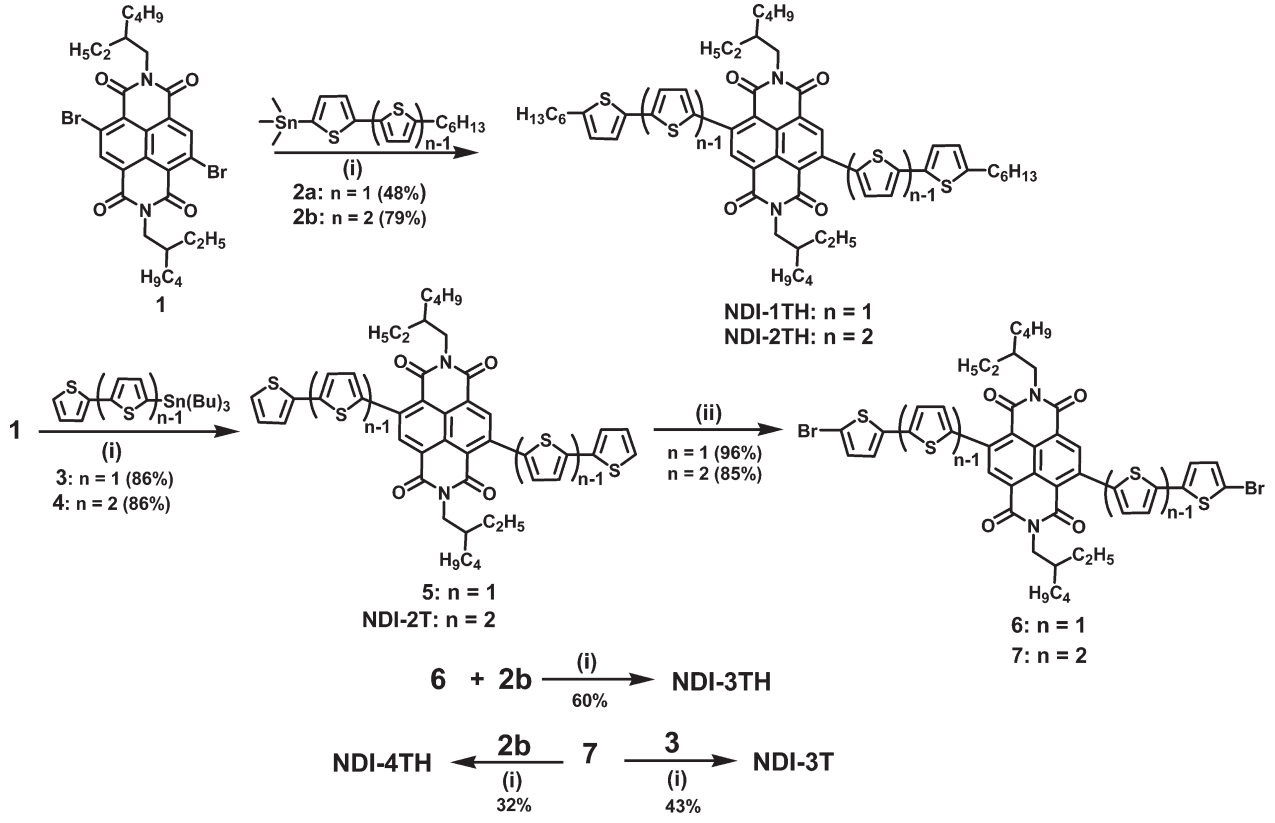

[a] Conditions: (i) $Pd(PPh_3)_4$, toluene, reflux; (ii) NBS, $CHCl_3$, DMF, 48 h, rt.

concentrated. The product was purified by column flash chromatography using a dichloromethane and hexane mixture. The pure product was collected and redissolved in chloroform and precipitated from methanol. The pure product was obtained as a dark green solid (216 mg, 43% yield). MALDI-TOF MS (m/z) calcd 982.2095, found 983.086 [$(M + H)^+$]. ^{1}H NMR (CD_2Cl_2, 300 MHz, ppm): δ 8.887 (s, 2H), 7.331−7.318 (m, 6H), 7.291 (dd, 2H), 7.242 (dd, 2H), 7.194 (dd, 2H), 7.105 (t, 2H), 4.108 (dd, 4H), 1.953−1.933 (m, 2H), 1.469−1.333 (m, 16H), 0.989−0.893 (m, 12H). ^{13}C NMR ($CDCl_3$, 500 MHz, ppm): δ 162.566, 140.474, 139.495, 139.305, 137.158, 136.976, 136.544, 135.517, 130.117, 127.981, 127.583, 125.417, 125.074, 124.789, 124.472, 123.961, 122.600, 79.528, 44.670, 37.804, 30.676, 28.614, 23.953, 23.144, 14.147, 10.641.

2.2. Characterization. ^{1}H NMR spectra were recorded on a Bruker AV300 at 300 MHz, whereas ^{13}C NMR spectra were recorded on a Bruker AV 500 at 500 MHz using $CDCl_3$ or CD_2Cl_2 as the solvent. Mass spectra were obtained with a Bruker Esquire LC/ion trap mass spectrometer, JEOL/HX-110, or a matrix-assisted laser desorption ionization time-of-flight (MALDI/TOF) instrument. Differential scanning calorimetry (DSC) analysis was performed on a TA Instruments Q100 under N_2 at a heating rate of 10 °C/min. Second-heating DSC scans are reported for all molecules except for NDI-1TH and NDI-2TH, where first-heating scans are reported. Thermogravimetric analysis of the NDI-nTH and NDI-nT was conducted on a Perkin-Elmer instrument, TGA 7. A heating rate of 5 °C/min under flow of N_2 was used with runs conducted from room temperature to 600 °C.

X-ray diffraction (XRD) data were collected from a Bruker-AXS D8 Focus diffractometer with Cu Kα beam (40 kV, 40 mA, λ = 0.15418 nm). Thin films for powder XRD were prepared by drop-casting from a concentrated (10 mg/mL) solution in chloroform onto glass slides or Si-wafers, followed by film annealing at 150 °C for 5 min. Cyclic voltammetry was measured on an EG&G Princeton Applied Research Potentiostat/Galvanostat (model 273A). Data were analyzed by model 270 electrochemical analysis system software on a PC computer. A three-electrode cell was used, using platinum wire electrodes as both the counter electrode and the working electrode. Silver/silver ion (Ag in 0.1 M $AgNO_3$ solution, Bioanalytical System, Inc.) was used as a reference electrode. Ferrocene/ferrocenium (Fc/Fc^+) was used as an internal standard. The potential values obtained in reference to Ag/Ag^+ were converted to the saturated calomel electrode (SCE) scale. All solutions were purged with N_2 for 20 min before each experiment. UV−vis absorption spectra were collected on a Perkin-Elmer model Lambda 900 UV/vis/near-IR spectrophotometer.

2.3. Fabrication and Characterization of Field-Effect Transistors. Organic field-effect transistors (OFETs) were fabricated in standard bottom-contact and bottom-gate geometry. Heavily n-doped silicon with 200 nm thermal oxide (C_0 = 17 nF/cm^2) acted as a gate electrode with a dielectric layer, as well as the substrate. Gold source and drain electrodes (~50 nm) with a thin chromium layer (~2 nm) were photolithographically patterned on the substrate. The width (W) and length (L) of the transistor channel are 800−1000 μm and 40−100 μm, respectively. The silicon dioxide surface was treated with octyltrichlorosilane (OTS-8). Thin films of NDI-nTH (or NDI-nT) were coated on the substrates by either spin-coating or thermal evaporation. NDI-nTH (or NDI-nT) solution (10 mg/mL) in 1,2-dichlorobenzene was spin-coated onto substrates at 1000 rpm for 60 s. The films were annealed at 120−200 °C for 10 min under a flow of nitrogen (<0.1 ppm traces of oxygen and moisture). Electrical characteristics were measured using an HP4145B semiconductor parameter analyzer in nitrogen atmosphere. The mobility was calculated from the saturation region of transfer curves

(I_{ds} vs V_g) at a source-drain voltage (V_{ds}) of ±80 V with the following equation: $I_{ds} = (\mu WC_0)(V_g - V_t)^2/(2L)$.

2.4. Fabrication and Characterization of Solar Cells. OPV devices were fabricated by spin-coating a 40 nm layer of poly(3,4-ethylenedioxythiophene):poly(styrene sulfonate) (PEDOT:PSS) onto ITO-coated glass substrates (10 Ω/□, Shanghai B. Tree Tech. Consult Co., Ltd., Shanghai, China) and drying them at 150 °C for 10 min under vacuum. NDI-*n*TH (or NDI-*n*T) solutions were prepared by dissolving 10 mg in each 1 mL of degassed chloroform at room temperature, and they were filtered with a 0.45 μm filter. The P3HT:NDI-*n*TH and P3HT:NDI-*n*TH blends were each spin-coated on top of the PEDOT:PSS layer at various speeds for 30 s to make a thin film of ~70 nm. The films were then annealed at 150 °C for 5 min. The substrates were taken out of the glovebox and loaded into a vacuum evaporator. A hole blocking layer (HBL) of 1,3,5-tris(4-phenylquinolin-2-yl)benzene (TQB) or 2,2′,2″-(1,3,5-benzinetriyl)tris(1-phenyl-1-H-benzimidazole) (TPBI) (3 nm) was thermally deposited on top of the active layer P3HT:NDI-*n*TH in a vacuum of 8×10^{-7} Torr. For the solar cell with a P3HT electron-blocking buffer layer, P3HT (8 mg/mL) in *o*-dichlorobenzene (ODCB) solution was spin-coated on top of the PEDOT:PSS layer, aged in a Petri dish for 5 min, and thermally annealed at 150 °C for 5 min to make a thin film of 15 nm. The P3HT:NDI-*n*TH blend was then spin-coated (70 nm) on top of the P3HT buffer layer in a glovebox. Finally, the cathode layer, which consists of LiF (1 nm) and Al (80 nm), was deposited onto the active layer or HBL layer using a shadow mask in a vacuum of 8×10^{-7} Torr. Each substrate contained five solar cells with an active area of 4.0 mm^2. Current−voltage characteristics were measured using an HP4155A semiconductor parameter analyzer (Yokogawa Hewlett-Packard, Tokyo) under 100 mW/cm^2 AM1.5 sunlight illumination from a filtered Xe lamp, calibrated using a NREL-calibrated Si diode.[29b] Film thickness was measured with an Alpha-Step 500 profilometer (KLA-Tencor, San Jose, CA). All measurements were done in ambient laboratory air.

The measurement of the external quantum efficiency or the incident photon to current efficiency (IPCE) was made using an Oriel xenon lamp (450 W) with an Oriel Cornerstone 130 1/8 m monochromator. The signal was measured with a calibrated standard silicon solar cell and a KG5 filter calibrated at NREL using a SR830 DSP lock-in amplifier at a chopping frequency of 400 Hz.

Atomic force microscopy (AFM) imaging was performed on the same solar cell devices using a Dimension 3100 SPM (Veeco) instrument operating in tapping mode. For transmission electron microscopy (TEM) imaging, thin films of the active layers were obtained by scratching edges of the device substrate. The device was then soaked in water until the thin film was peeled-off from the device substrate. The films were supported on TEM grids (Electron Microscopy Sciences) for bright-field transmission electron microscopy (BF-TEM) imaging. An FEI Tecnai G^2 F20 TEM at 200 kV was employed, and images were acquired with a CCD camera and recorded with Gatan Digital Micrograph software.

3. RESULTS AND DISCUSSION

3.1. Synthesis and Characterization. The synthesis of the oligothiophene-functionalized NDI molecules, NDI-*n*TH and NDI-*n*T, is outlined in Scheme 1. 2,6-Dibromonaphthalene diimide (**1**),[45] 5-hexyl-2-trimethylstannylthiophene (**2a**),[46a] 5-hexyl-2-trimethylstannylbithiophene (**2b**),[46a] and 2-trimethylstannylbithiophene (**3**)[46b] were made according to reported methods. Stille coupling of compound **1** with **2a** or **2b** afforded NDI-1TH and NDI-2TH as a red solid and a blue solid in 48 and 79% yields, respectively. Stille coupling of **1** and 2-trimethylstannylthiophene (**3**) gave compound **5** as a red solid in 86%

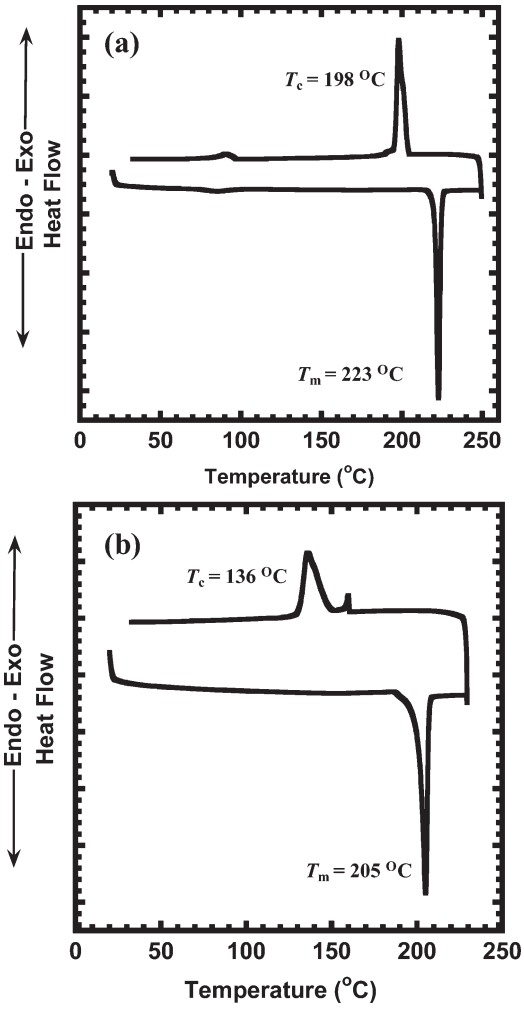

Figure 2. Second-heating DSC scans of (a) NDI-3TH and (b) NDI-4TH at a heating/cooling rate of 10 °C/min in nitrogen.

yield, whereas NDI-2T was obtained as a blue solid in 86% yield by Stille coupling of compounds **1** and **4**. Bromination of compounds **5** and NDI-2T using NBS gave precursors **6** and **7** in high yields. Stille couplings of **6** and **2b**, **7** and **2b**, and **7** and **3** gave NDI-3TH, NDI-4TH, and NDI-3T as dark green solids in 60, 32, and 43% yields, respectively. All final compounds were purified by column flash chromatography and recrystallized from chloroform/methanol solvent mixtures. The molecular structures of the six molecules were confirmed by ^1H NMR, ^{13}C NMR, high-resolution mass spectroscopy, or MALDI. Single-crystal X-ray structure of some of the NDI-*n*TH molecules (NDI-3TH and NDI-4TH) was also determined. All oligothiophene-functionalized NDIs are readily soluble in organic solvents including chloroform, toluene, and chlorobenzene.

Thermogravimetric analysis (TGA) was used to assess the thermal stability of the oligothiophene-functionalized NDIs. The TGA scans of NDI-*n*TH and NDI-*n*T (Figure S1 in the Supporting Information) showed that all six molecules were stable to temperatures above 300 °C, with onset decomposition temperatures (T_D) in the range 336−348 °C. The observed T_D values are significantly higher than those of the corresponding oligothiophenes with or without an alkyl chain.[47a] For example,

dx.doi.org/10.1021/cm2019668 |*Chem. Mater.* 2011, 23, 4563–4577

Table 1. Thermal, Optical, and Electrochemical Properties of NDI-*n*TH and NDI-*n*T

comp.	T_D (°C)	T_m/T_c (°C)	$\lambda_{max}^{a,b}$ (nm)	$\lambda_{max}^{a,c}$ (nm)	E_g^{opt} (eV)	E_{ox}^{onset} (V)	E_{red}^{onset} (V)	IP (eV)	EA (eV)	E_g^{el} (eV)
NDI-1TH	338	74	525	528	2.06	1.66	−0.43	6.06	3.97	2.09
NDI-2TH	338	109	604	628	1.59	1.31	−0.37	5.71	4.03	1.68
NDI-3TH	336	223/198	632	654	1.57	1.13	−0.35	5.53	4.05	1.48
NDI-4TH	340	205/136	638	801	1.39	1.06	−0.267	5.46	4.13	1.33
NDI-2T	342	183/110	570	609	1.72	1.43	−0.285	5.83	4.12	1.71
NDI-3T	348	204/116	607	683	1.41	1.19	−0.256	5.60	4.14	1.46

[a] Lowest energy absorption maximum. [b] Absorption in dilute chloroform solution. [c] Thin film absorption.

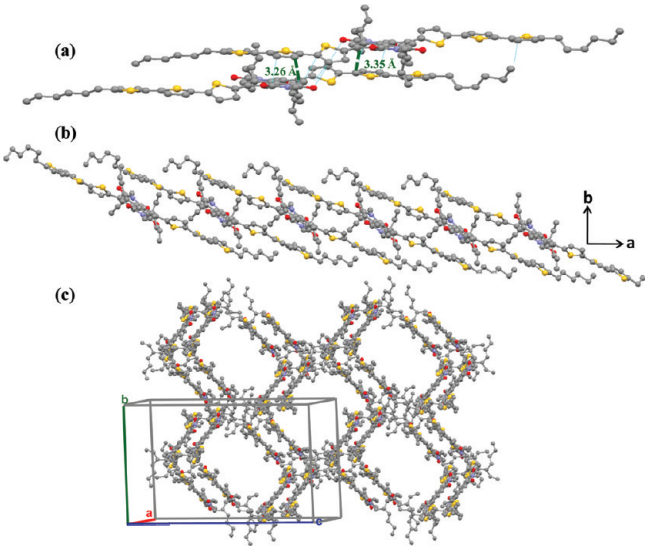

Figure 3. (a) π-stacking of two NDI-3TH molecules with the shortest intermolecular distance of 3.26 Å. (b) Molecular packing of NDI-3TH, illustrating a slipped π-stacking along the *a*-axis. (c) Molecular packing of NDI-3TH in a unit cell.

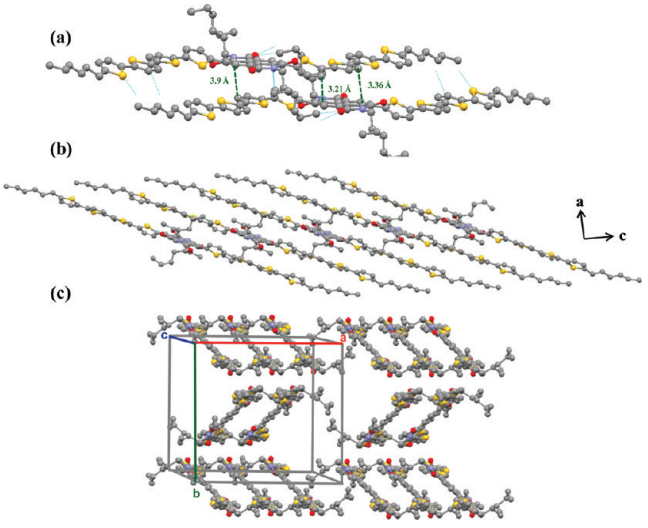

Figure 4. Molecular packing structures of NDI-4TH illustrating (a) π-stacking of two NDI-4TH molecules with the shortest intermolecular distance of 3.21 Å, (b) a slipped π-stacking along the *c*-axis, and (c) NDI-4TH in a unit cell.

α-sexithiophene (309 °C)[47a] and its dihexyl derivative (310 °C)[47a] have lower T_D values than NDI-*n*TH and NDI-*n*T.

The thermal transition properties of the oligothiophene-functionalized NDIs were also investigated by differential scanning calorimetry (DSC). The second-heating DSC scans of NDI-*n*TH and NDI-*n*T are exemplified by those of NDI-3TH and NDI-4TH in Figure 2; the DSC scans of the others are given in Figure S2 in the Supporting Information. The melting transition temperature (T_m) and corresponding recrystallization temperature (T_c) are summarized in Table 1. The T_m increased from 74 °C in NDI-1TH to 223 °C in NDI-3TH and then decreased slightly to 205 °C in NDI-4TH. The T_m of the NDI-*n*TH series thus increases with molecular weight to a peak at $n = 3$. NDI-2TH with hexyl end groups has a significantly lower melting transition (109 °C) compared to that of NDI-2T without hexyl end groups (183 °C). In contrast, NDI-3TH has a melting transition comparable to that of NDI-3T (Table 1). The NDI materials showed clear thermal transitions during the cooling from the melt, except for NDI-1TH and NDI-2TH, which did not exhibit any recrystallization transition in the cooling scan, suggesting relatively slow crystallization rates in these latter materials. The observed melting temperature (T_m) in these oligothiophene-functionalized NDI materials (Table 1) is lower compared to that of the corresponding oligothiophenes with or without dihexyl end groups. For example, α-quarterthiophene (221 °C)[47a] and its dihexyl derivative (179 °C),[47b] as well as α-sexithiophene (280 °C)[47c] and its dihexyl derivative (290 °C),[47c] have higher T_m values. On the other hand, the T_m values of the present π-conjugated oligomers NDI-*n*TH and NDI-*n*T are much higher than those of NDIs that have only alkyl substitutions at the imide nitrogens and no extension of conjugation through functionalization of the naphthalene ring.[40b,47d]

3.2. Single-Crystal Structures. The solid state packing and intermolecular interactions in the NDI-*n*TH series of molecules were investigated by X-ray diffraction on single-crystals of NDI-3TH and NDI-4TH. The NDI-3TH single-crystals were grown from a chloroform/methanol solution, whereas NDI-4TH single-crystals were grown from a chloroform solution. The resulting single crystal structure of NDI-4TH was of good quality, whereas the refinement of the NDI-3TH crystal structure was of poor quality as a result of the flexible belt-like single-crystals; however, the crystal structure of NDI-3TH is also presented because it can still be used for illustration and comparison purposes. Single crystal X-ray diffraction of NDI-3TH shows a monoclinic primitive lattice with a space group of $P121/c1$ and unit cell dimensions of $a = 10.3066(15)$ Å, $b = 18.779(3)$ Å, $c = 31.399(5)$ Å, $\alpha = 90°$, $\beta = 92.774(9)°$, and $\gamma = 90°$. The NDI-4TH crystal structure also shows a monoclinic primitive lattice with a space group of $P121/c1$ and unit cell dimensions of $a = 20.041(3)$ Å, $b = 16.808(3)$ Å, $c = 9.9175(13)$ Å, $\alpha = 90°$, $\beta = 100.606(5)°$, and $\gamma = 90°$. The NDI core in NDI-3TH and NDI-4TH shows a

dx.doi.org/10.1021/cm2019668 |*Chem. Mater.* 2011, 23, 4563–4577

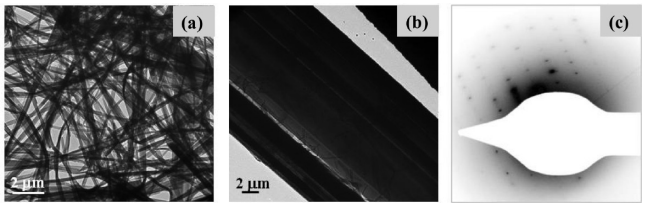

Figure 5. TEM image of self-assembled NDI-3TH nano/microwires: (a) large area of the nanowires; (b) a TEM image of a single microwire; and (c) the corresponding electron diffraction of the microwire in Figure 5b.

relatively planar geometry (Figures 3 and 4). Interestingly, the thiophene rings adjacent to the NDI core exhibit a *syn* configuration in both NDI-3TH and NDI-4TH molecules, while the outer thiophene rings exhibit an *anti* configuration. This kind of orientation appears to be directed by the carbonyl groups in the NDI core to facilitate hydrogen bonding (Figures 3a and 4a). The oligothiophene blocks in NDI-4TH adopt a more planar configuration relative to the NDI core, compared to the oligothiophene rings in NDI-3TH. Each of the thiophene rings adjacent to the NDI core has a twist angle of 35° in NDI-3TH. The *syn* configurations of the inner thiophene rings in NDI-3TH have a relatively large dihedral angle of 40°, whereas the *anti* configurations of the outer thiophene rings have a smaller dihedral angle (20°). In contrast, each of the thiophene rings adjacent to the NDI core in NDI-4TH has a much smaller twist angle (25°). The thiophene rings in NDI-4TH exhibit *syn*, *anti*, and *anti* configurations with dihedral angles of 23, 7, and 12°, respectively.

The crystal structures of both of these NDI-*n*TH molecules show that there is no orbital overlap between the naphthalene diimide cores. The bulky ethylhexyl side chains on the NDI core prevent optimum orbital overlap between neighboring NDIs. The N···N distance between two adjacent NDI units in NDI-3TH is 10.31 Å, whereas the same distance in NDI-4TH is slightly shorter (9.92 Å). The π-stacking is mainly between the naphthalene diimide units and the thiophene rings. Figures 3a and 4a show that the π-stacking between two adjacent molecules in NDI-3TH and NDI-4TH with the shortest intermolecular distance are 3.26 and 3.21 Å, respectively. NDI-3TH forms a slipped face-to-face π-stacking along the *a*-axis as shown in Figure 3b. Similarly, NDI-4TH forms a slipped face-to-face π-stacking along the *c*-axis as shown in Figure 4b. Figure 3c shows that there are four NDI-3TH molecules in a unit cell. In contrast, there are only two NDI-4TH molecules in a unit cell, forming a zigzag structure, as shown in Figure 4c.

3.3. Self-Assembly of NDI-*n*TH Nanowires. Unlike perylene diimides (PDIs) and other π-conjugated planar molecules whose solution-phase self-assembly into nanowires and other one-dimensional (1-D) nanostructures has been extensively investigated,[30,48,49] 1D nanostructures of naphthalene diimides (NDIs) and their self-assembly have not been reported. Because such nanowires and related 1D nanostructures represent one approach to the rational control of the morphology of BHJ polymer solar cells,[9,29−32] we have done an initial investigation of the solution-phase assembly of nanowires from NDI-*n*TH.

We selected NDI-3TH for the investigation of solution-phase self-assembly and used the solvent-exchange method,[30] where single-crystal nano/microwires were prepared by adding methanol (a nonsolvent) to a solution (5 mg/mL) of NDI-3TH in dichloromethane, and the resulting mixtures were left for two

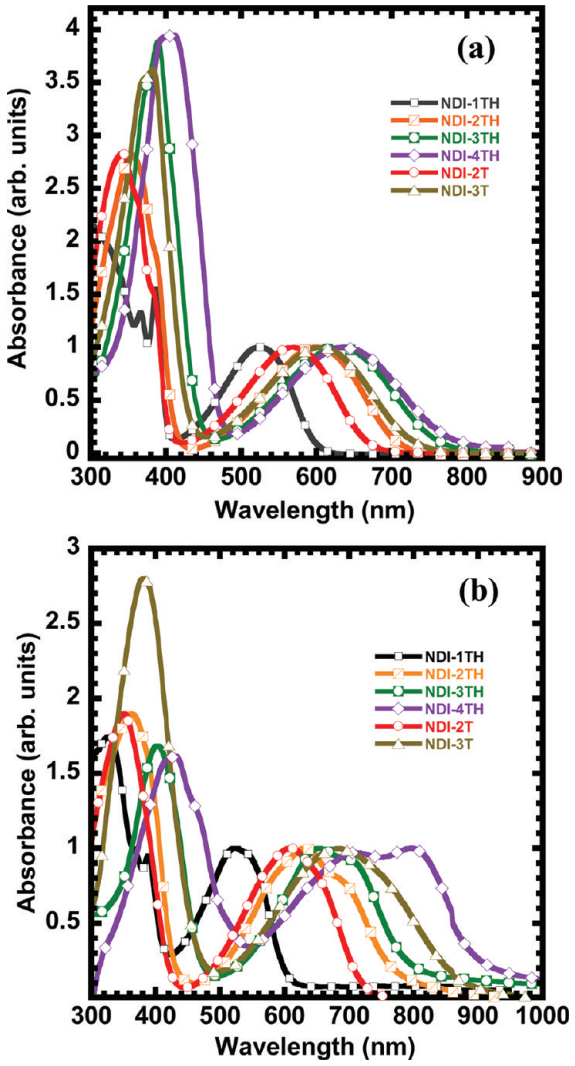

Figure 6. Optical absorption spectra of NDI-*n*TH and NDI-*n*T: (a) in dilute chloroform solutions and (b) as thin films.

weeks.[48e] Figure 5 shows the transmission electron microscopy (TEM) images of NDI-3TH nanowires. The width or diameter of the nano/microwires was polydisperse (100 nm to 20 μm), and the length was in the 1−300 μm range (Figure 5a). A single TEM image of a single microwire of NDI-3TH (13 μm width) and the corresponding electron diffraction of the single microwire are shown in Figure 5b and c. The selected area electron diffraction (SAED) pattern (Figure 5c) indicates that the nano/microwires are single crystalline. To further investigate the solid state morphology of these NDI-3TH nanowires/microwires, we performed X-ray diffraction (XRD) analysis on drop-casted films from methanol dispersion of the nanowires, (Figure S3 in the Supporting Information). The X-ray diffraction patterns of the nanowire films show strong diffraction peaks at 2θ = 4.90, 10.4, 15.9, 18.3, and 21.5°, corresponding to the *d*-spacing of 18.0, 8.5, 5.56, 4.84, and 4.14 Å. These intense and sharp diffraction peaks suggest that the nanowire films are highly crystalline and oriented. The *d*-spacing of 18.0 Å can be assigned to the [010] direction based on the previously discussed single crystal X-ray structure.

dx.doi.org/10.1021/cm2019668 |*Chem. Mater.* 2011, 23, 4563–4577

It is remarkable that single-crystalline ultralong nanowires can be assembled from NDI-3TH given the bulky ethylhexyl side chains and hexyl end groups of the molecule, as well as the observed impeded intermolecular interactions between the NDI units (Figure 3) and the slipped face-to-face π-stacking. These results suggest that ultralong single crystalline nano-/microwires of oligothiophene-functionalized naphthalene diimides can be assemble from solution. Further study and optimization of the assembly conditions will be essential to control the width and aspect ratio in the ranges of particular interest in nanowire-based bulk heterojunction OPVs.[9,29,30]

3.4. Photophysics. The photophysics and light harvesting potential of oligothiophene-functionalized NDIs, NDI-*n*TH and NDI-nT, were investigated by absorption spectroscopy of the molecules in dilute solution and as thin films. Figure 6a shows the absorption spectra of NDI-*n*TH and NDI-*n*T in dilute chloroform solutions ($(2-5) \times 10^{-6}$ M). The absorption maxima (λ_{max}) of the six molecules are summarized in Table 1. In solution, the NDI molecules show two absorption bands: a $\pi-\pi^*$ transition in the 300−480 nm range and an intramolecular charge transfer (ICT) band in the 480−780 nm range. A significant red shift in the absorption maximum is observed as the number of thiophene rings increased. A bathochromic shift of 79−113 nm in λ_{max} was observed as the size of the oligothiophene appended to NDI increased from $n = 1$ (NDI-1TH) to $n = 2$ (NDI-2TH) and to $n = 4$ (NDI-4TH). Interestingly, both NDI-3TH and NDI-4TH have a similar λ_{max} in solution (632 and 638 nm), suggesting that the conjugation length in NDI-4TH has reached a plateau. The λ_{max} in NDI-2T and NDI-3T in chloroform solution are similar to those of NDI-2TH and NDI-3TH, which confirms the similarity of the electronic structure between the alkyl substituted and unsubstituted end groups.

The absorption spectra of the NDI molecules as thin films are shown in Figure 6b, and the λ_{max} and optical band gap (E_g^{opt}) are summarized in Table 1. The absorption spectra of some of the NDI-*n*TH thin films show some vibronic structures, whereas the absorption spectra of NDI-*n*T materials were featureless. The λ_{max} in NDI-*n*TH and NDI-*n*T thin films varied from 528 nm in NDI-1TH to 801 nm in NDI-4TH. The optical band gap (E_g^{opt}) of the oligothiophene-functionalized NDI materials varied from 2.1 eV in NDI-1TH and 1.6 eV in NDI-3TH to 1.4 eV in NDI-4TH and NDI-3T (Table 1). The large red shift in the absorption maximum with increasing oligothiophene size (n) is evidence of the increase in the intramolecular charge transfer (ICT) and, thus, conjugation length in these donor−acceptor−donor molecules.[39] It is also clear that, as the oligothiophene size increased, the difference between the λ_{max} in solution and thin film steadily increased, which suggests that the increase in oligothiophene size leads to enhanced intermolecular interactions and long-range 2D order in the NDI-*n*TH and NDI-*n*T materials. For example, the λ_{max} in NDI-*n*TH (n = 1, 2, 3) and NDI-2T thin films was only slightly red-shifted (3−39 nm) compared to the λ_{max} in dilute solution. In contrast, the λ_{max} values in NDI-4TH and NDI-3T thin films showed large bathchromic shifts (76 and 163 nm) compared to the respective λ_{max} values in solution. In the NDI-4TH thin film, the absorption maximum was red-shifted by 147 nm compared to that of NDI-3TH, despite their similar λ_{max} values in solution. The large red shift in thin film absorption compared to solution spectra can be attributed to the improved planarization of the molecular backbone in the solid state that results in enhanced ICT and intermolecular interactions.

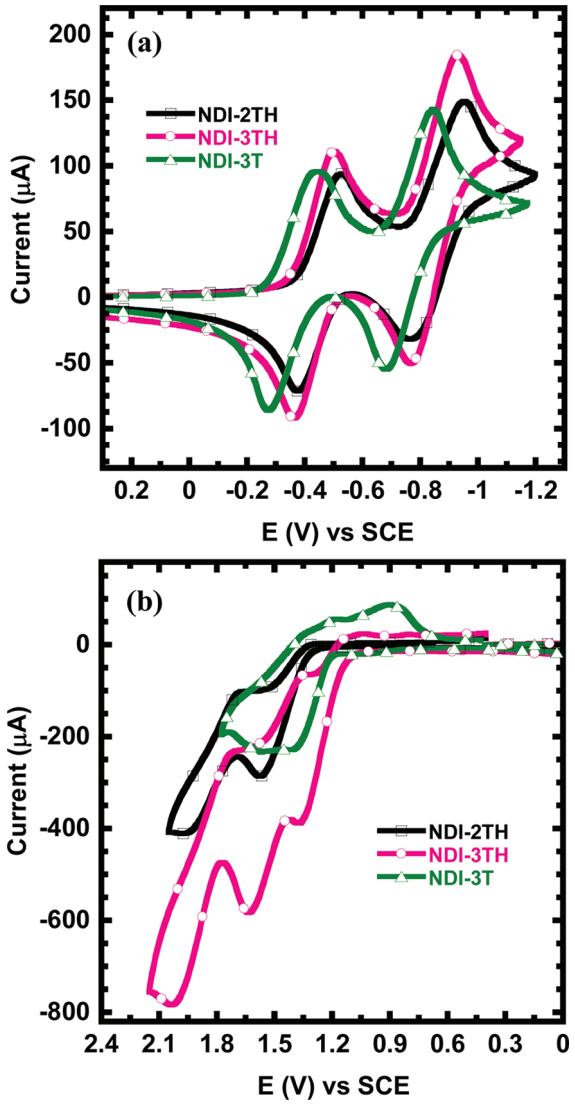

Figure 7. Cyclic voltammograms of NDI-*n*TH (n = 2, 3) and NDI-3T (1−1.5 mM) in benzene/acetonitrile (10:3 v/v), 0.1 M $TBPF_6$: (a) reduction waves and (b) oxidation waves at a scan rate of 150 mV/s.

These results on the photophysics of the NDI-*n*TH and NDI-*n*T materials demonstrate that their absorption spectra and optical band gaps are such that they can contribute to substantial light harvesting and exciton generation in OPVs. Extension of the absorption bands of these candidate acceptor materials to the near-IR range (700−950 nm) suggests that there is latitude in the selection of a candidate donor polymer for pairing with them in BHJ solar cells. To achieve complementary light harvesting, a donor polymer with an absorption band in the 420−600 nm spectral range would be ideal.

3.5. Electrochemical Properties. The HOMO/LUMO energy levels and associated ionization potential (IP)/electron affinity (EA) of the NDI-*n*TH and NDI-*n*T molecules are critical to fully evaluating their potential as acceptor materials in OPVs. We estimated the HOMO/LUMO energy levels by performing cyclic voltammetry of the NDI molecules in 1.0−1.5 mM solutions in benzene/acetonitrile mixture (10:3 v/v).

Representative cyclic voltammograms (CVs) of the NDI molecules are shown in Figure 7a. All six molecules showed

dx.doi.org/10.1021/cm2019668 |*Chem. Mater.* 2011, 23, 4563–4577

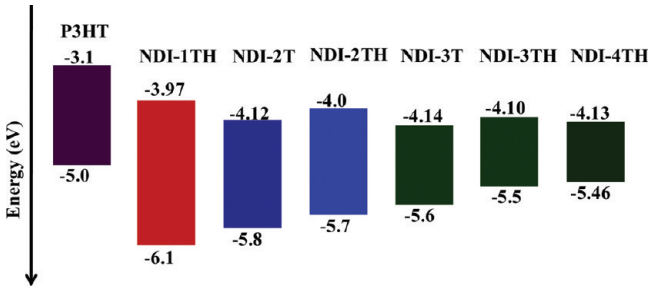

Figure 8. HOMO/LUMO energy levels of oligothiophene-functionalized NDIs compared to those of P3HT.

two reversible reduction waves with onset reduction potentials of −0.43 to −0.256 V (vs SCE). The estimated electron affinity (EA) values, or LUMO energy levels (EA = E_{red}^{onset} + 4.4 eV),[50] were in the range −3.97 to −4.14 eV for the series of six NDI molecules (Table 1). The similarity of the LUMO level (∼−4.0 eV) of all the NDI-*n*TH and NDI-*n*T molecules is to be expected from the constant NDI core unit in the materials. These LUMO levels of NDI-*n*TH and NDI-*n*T are comparable to the literature values reported for various NDI-based small molecules[40−42] and polymers.[43−45]

The observed oxidation CVs in Figure 7b and Figure S4 in the Supporting Information clearly show irreversible oxidation waves for all of the NDI molecules except NDI-2T and NDI-3T, which are quasi-reversible. The reason for the quasi-reversible oxidation of NDI-*n*T without hexyl end groups, whereas the oxidation of NDI-*n*TH with hexyl end groups is completely irreversible, is not obvious but may be related to the delocalization of the radical cation into the α-carbons of the hexyl end groups. As expected, the main feature of the oxidation CV is that the oxidation potential progressively became less positive with increasing oligothiophene size in the NDI-*n*TH and NDI-*n*T molecules. The onset oxidation potentials (E_{ox}^{onset}) thus decreased from 1.66 V in NDI-1TH to 1.06 V (versus SCE) in NDI-4TH (Table 1). The estimated ionization potential (IP) values, or HOMO energy levels (IP = E_{ox}^{onset} + 4.4 eV),[50] thus varied from −6.06 eV for NDI-1TH to −5.46 eV for NDI-4TH (Table 1). These results clearly demonstrate that the HOMO level can be varied by 0.6 eV by varying the oligothiophene size in the oligothiophene-functionalized NDI molecules.

The trends in measured HOMO/LUMO energy levels of NDI-*n*TH and NDI-*n*T materials are graphically illustrated in Figure 8 along with the reported HOMO/LUMO energy levels of poly(3-hexylthiophene) (P3HT), a common donor polymer semiconductor widely used in BHJ solar cells. The LUMO level of −4.0 to −4.1 eV observed in these NDI molecules is remarkable comparable to LUMO levels reported for various fullerene acceptors (−3.8 to −4.5 eV for $PC_{61}BM$ or $PC_{71}BM$).[38] On the basis of the criterion of HOMO/LUMO energy levels and their offsets relative to a donor polymer, as discussed earlier, we can thus conclude that the series of NDI molecules have potential as acceptor materials for OPVs. For example, if P3HT is the donor, ΔE_{LUMO} ∼ 0.8 eV and ΔE_{HOMO} ∼0.5−1.1 eV, which are greater than the target 0.3 eV. The observed LUMO levels of the NDI-*n*TH and NDI-*n*T molecules suggest that electron transport should be feasible in the materials. However, we note that the low ionization potential (5.5−5.6 eV) of some of these materials (NDI-3T, NDI-3TH, NDI-4TH) suggests that they could also transport holes, a feature of organic semiconductors with

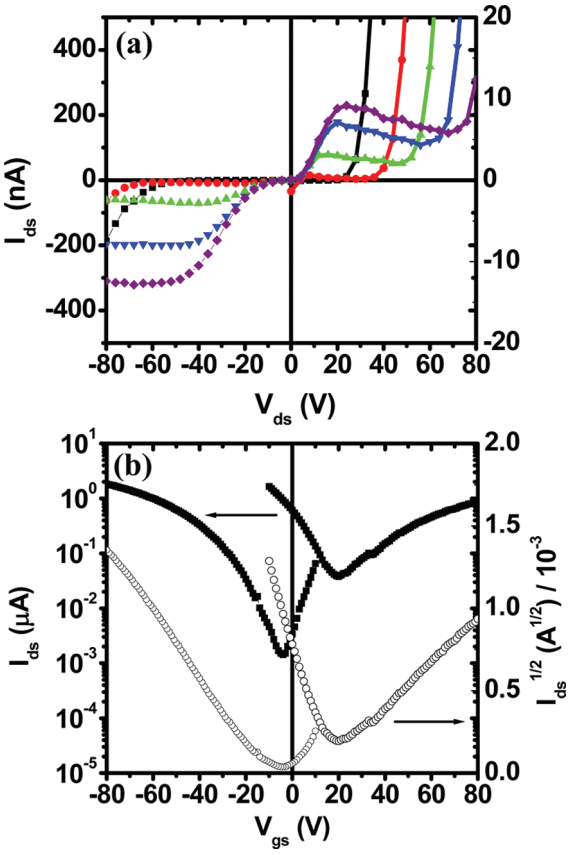

Figure 9. (a) Output and (b) transfer characteristics of spin-coated NDI-4TH thin film transistors (W/L = 20).

donor−acceptor architecture.[44,51] It is interesting that the observed electrochemical band gap (E_g^{el}), or transport gap, of these NDI materials, which varies from 1.3 eV in NDI-4TH to 2.1 eV in NDI-1TH (Table 1), is very close to the optical band gap (E_g^{opt}). In fact, E_g^{el} is either identical to E_g^{opt} (e.g., NDI-1TH, NDI-4TH, NDI-2T, NDI-3T) or is larger by less than 100 meV. The implication of this is that the binding energy of excitons in these oligothiophene-functionalized NDI materials is small compared to the typical 0.5−1.0 eV expected in most organic semiconductors.[52]

3.6. Charge Transport. We investigated the charge transport properties of the NDI-*n*TH and NDI-*n*T by using a bottom-contact and bottom-gate field-effect transistor geometry with an octyltrichlorosilane (OTS) treated silicon dioxide dielectric and patterned gold/source drain electrodes. The substrates were at room temperature during the film deposition via spin coating or in the case of NDI-1TH and NDI-2TH by evaporation. Films of NDI-1TH and NDI-2TH could not be made by spin coating from solution because of the hydrophobic OTS-treated surface, which led to poor film wetting; therefore, evaporated films were evaluated. Field effect charge transport could not be observed in NDI-1TH, which may be due to its rapid crystallization into large domain aggregates (Figure S5 in the Supporting Information). The devices were briefly exposed to air while transferring them from the device fabrication facility to the nitrogen-filled device testing box. Both field-effect electron transport and hole transport were observed in all NDI-*n*TH and NDI-*n*T materials except NDI-1TH. Typical output and transfer characteristics of NDI-*n*TH OFETs are exemplified by those of NDI-4TH in Figure 9.

dx.doi.org/10.1021/cm2019668 |*Chem. Mater.* 2011, 23, 4563–4577

Table 2. Field-Effect Charge Transport Properties of NDI-*n*TH and NDI-*n*T

	n-channel			p-channel			
comp.	μ_e (cm^2/V s)	I_{on}/I_{off}	V_t (V)	μ_h (cm^2/V s)	I_{on}/I_{off}	V_t (V)	μ_e/μ_h
NDI-2TH[a]	5.0×10^{-6}	10^2	17.4	1.3×10^{-4}	10^3	−23.3	0.04
NDI-3TH	6.9×10^{-4}	10^3	−5.4	2.5×10^{-4}	10^2	−7.2	2.76
NDI-4TH[b]	9.0×10^{-4}	10	16.7	2.1×10^{-3}	10^2	−13.2	0.43
NDI-2T	5.1×10^{-4}	10^3	4.5	2.2×10^{-5}	10^2	−26.9	23.2
NDI-3T[c]	1.5×10^{-4}	10^2	20.3	1.5×10^{-4}	10^2	−21.6	1.0

[a] Thermally evaporated film. [b] Annealed at 150 °C. [c] Annealed at 120 °C.

The carrier mobilities (μ_h and μ_e), current on/off ratios (I_{on}/I_{off}), and threshold voltages (V_{th}) data for OFETs based on the five NDI materials are summarized in Table 2.

In general, as expected from their favorable LUMO energy levels (−4.0 to −4.1 eV), the NDI-*n*TH and NDI-*n*T materials transport electrons with moderately high mobility that varies from 5.0×10^{-6} $cm^2/(V\ s)$ in NDI-2TH films to 9.0×10^{-4} $cm^2/(V\ s)$ in NDI-4TH films (Table 2). In fact, the field-effect mobilities of electrons in all spin coated films of NDI-*n*TH and NDI-*n*T are sufficiently high ($(1.5-9.0) \times 10^{-4}$ $cm^2/(V\ s)$) to meet one of the previously discussed design criteria for new *non-fullerene* acceptors for OPVs. However, hole transport in all of the oligothiophene-functionalized NDI materials is equally fairly high, with field-effect mobility of holes varying from 2.2×10^{-5} $cm^2/(V\ s)$ in NDI-2T to 2.1×10^{-3} $cm^2/(V\ s)$ in NDI-4TH (Table 2). Among the series of NDI materials, NDI-4TH has the highest electron mobility and also has an even higher hole mobility, effectively making it a p-type semiconductor. By looking at the electron/hole mobility ratio (μ_e/μ_h), we find that the majority carriers are electrons in two of the materials (NDI-3TH and NDI-2T), holes in two of them (NDI-4TH and NDI-2TH), and perfectly balanced ambipolar transport in NDI-3T (Table 2). These charge transport results suggest that some of the NDI-*n*TH and NDI-*n*T materials may not be very effective acceptor materials for OPVs by virtue of the majority carriers being holes, despite their favorable LUMO energy levels (−4.0 to −4.1 eV).

We note that the I_{on}/I_{off} ratio is low (10^1-10^3) for all of the oligothiophene−NDI materials. The low I_{on}/I_{off} ratio is commonly seen in ambipolar OFETs where the majority charge carriers of the operation are determined by the applied voltage at the electrodes, that is, electrons for the n-channel mode with a positive voltage or holes for the p-channel mode with a negative bias.[44,53] The low on−off current ratio comes from the relatively high off-current (I_{off}). I_{on} in OFETs under a high gate voltage is mainly governed by the field-effect mobility of the majority charge carriers. However, in an off-state of an ambipolar OFET with a low gate voltage, I_{off} is often increased by the action of minority charge carriers, that is, holes (electrons) for the n-channel (p-channel) mode, which can be easily injected to the corresponding electronic energy level of the ambipolar semiconductor. This feature is not observed in unipolar OFETs where minority charge carriers are not active.

3.7. Non-fullerene Bulk Heterojunction Solar Cells. The potential of the new NDI-based semiconductors NDI-*n*TH and NDI-*n*T, as acceptor materials in OPVs, was investigated by using P3HT as the donor in bulk heterojunction (BHJ) solar cells. As previously discussed (Figure 8), the HOMO/LUMO

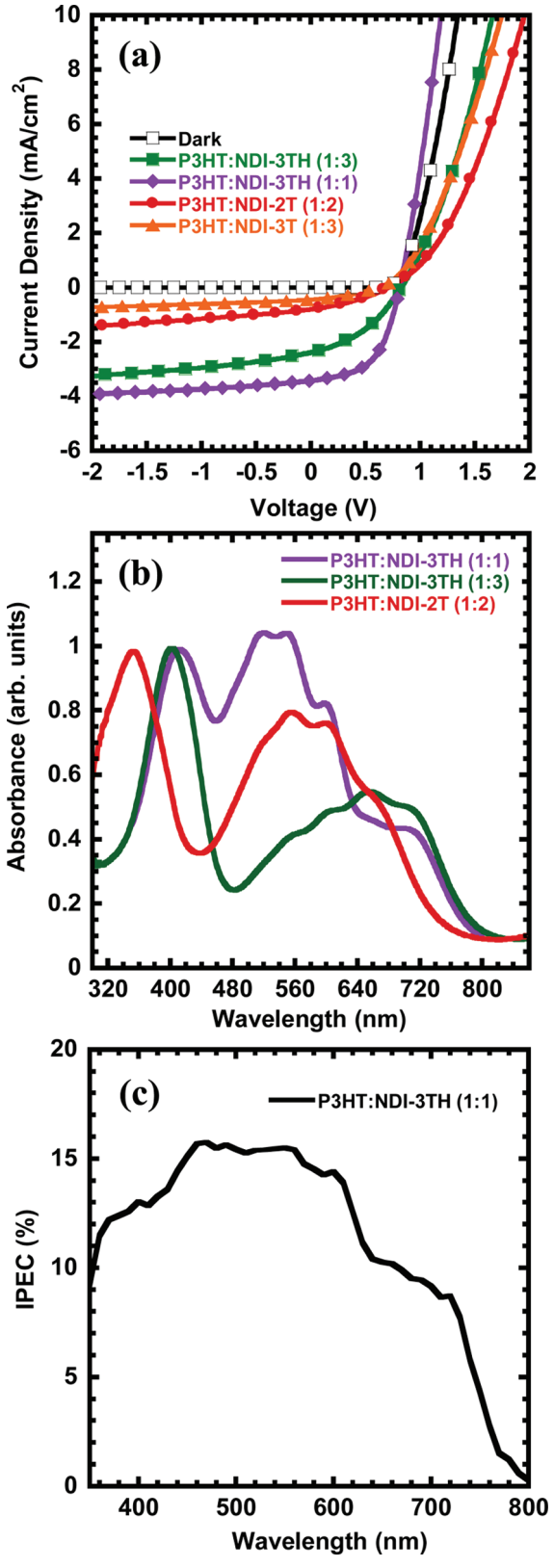

Figure 10. (a) Current density−voltage curves of P3HT:NDI-*n*TH or P3HT:NDI-*n*T photodiodes under 100 mW/cm^2 sunlight illumination; (b) absorption spectra of P3HT:NDI-3TH (or P3HT:NDI-2T) blend films on glass/ITO/PEDOT:PSS substrate; and (c) IPCE spectrum of P3HT:NDI-3TH (1:1) solar cell with 1.5% PCE.

dx.doi.org/10.1021/cm2019668 |*Chem. Mater.* 2011, 23, 4563–4577

energy levels of each of the NDI materials provide good band offsets with those of P3HT. Photodiodes with a device architecture of ITO/PEDOT:PSS/P3HT:NDI-*n*T(H)/HBL/LiF/Al were fabricated and characterized, where the thin layer of 1,3,5-tris(4-phenylquinolin-2-yl)benzene (TQB)[54] or 2,2′,2″-(1,3,5-benzinetriyl)-tris(1-phenyl-1-H-benzimidazole) (TPBI)[50a] was inserted between the active layer and the cathode as a hole-blocking layer to improve the overall device performance. Incorporation of a hole-blocking layer (HBL) between the active layer and the cathode electrode is well-known in bilayer solar cells and serves as an exciton blocking layer that prevents exciton quenching at the acceptor/cathode interface, thus leading to an increase in fill factor (*FF*) and short-circuit current density (J_{sc}).[5b] Among the six semiconductors, only NDI-3TH, NDI-2T, and NDI-3T showed a photovoltaic response. It is interesting to note that each of the three NDI materials that did not show a photovoltaic response in BHJ blends with P3HT has holes as the majority carriers with $\mu_e/\mu_h < 1$ (Table 2). In this respect, the lack of photovoltaic response in NDI-4TH is particularly noteworthy because it has the highest electron and hole mobilities among the series of NDI-based semiconductors. This is an important result in that it highlights and clarifies the criterion of charge transport in the design of acceptor materials; that is, the majority carriers in the acceptor material should be electrons.

The current density voltage (*J*—*V*) curves of the P3HT:NDI-3TH (1:3), P3HT:NDI-2T (1:2), and P3HT:NDI-3T (1:3) BHJ solar cells under dark and under 100 mW/cm^2 AM1.5 solar illumination are shown in Figure 10a. The photovoltaic parameters calculated from the current density−voltage (*J*−*V*) curves, including open-circuit voltage (V_{oc}), short-current (J_{sc}), and fill factor (*FF*), are summarized in Table 3. The variation of the V_{oc} from 0.83 V in the P3HT:NDI-3TH system to 0.71 V in P3HT:NDI-2T and 0.64 V in P3HT:NDI-3T cannot be fully understood on the basis of the differences in the HOMO energy level of P3HT and the LUMO levels of these acceptor materials, which are essentially constant ($\Delta E_{HOMO/LUMO}$ = 0.9−1.0 eV). In the case of P3HT/fullerene BHJ solar cells, it is known that the V_{oc} can also vary considerably, which has been explained by factors such as the scale of the two-phase morphology,[33] charge transport,[9b,29a,33a] and blend compositions.[9b,29a] BHJ solar cells based on the NDI-3TH acceptor gave the highest power conversion efficiency (PCE) of 0.77%, with a high V_{oc} of 0.83 V, J_{sc} of 2.39 mA/cm^2, and *FF* of 0.39 under 100 mW/cm^2 AM1.5 solar illumination in air. The photovoltaic efficiency was significantly lower in the case of NDI-3T (0.09% PCE) and NDI-2T (0.19% PCE), despite the similarity of the electron mobilities of NDI-2T and NDI-3TH. This means that the observed trends in photovoltaic efficiency cannot be explained solely by charge transport and carrier mobilities. Additional factors such as morphology and light absorption may also contribute to the observed trends in photovoltaic efficiency.

Examination of the effect of the BHJ blend composition showed that a 1:3 weight ratio gave the best performances in P3HT:NDI-3TH and P3HT:NDI-3T, whereas the optimum composition was 1:2 for P3HT:NDI-2T. The optimum composition in P3HT/fullerene BHJ solar cells was found to be 1:1.[55] Both the NDI-based acceptor and the P3HT in the present BHJ solar cells significantly contribute to light harvesting, as exemplified by the blend absorption spectra in Figure 10b. The absorption of the blend films clearly shows that P3HT:NDI-3TH blends harvest more of the 640−800 nm light than the P3HT:NDI-2T blends, which can partly explain the superior performance of the NDI-3TH photodiodes.

Table 3. Properties of BHJ Polymer Solar Cells

comp.	J_{sc} (mA/cm^2)	V_{oc} (V)	*FF*	η_{avg} (η_{max}) (%)
P3HT:NDI-3TH (1:3)[a]	2.39	0.83	0.39	0.73 (0.77)
P3HT:NDI-2T (1:2)[b]	0.81	0.71	0.34	0.17 (0.19)
P3HT:NDI-3T (1:3)[b]	0.45	0.64	0.33	0.09 (0.09)
P3HT:NDI-3TH (1:1)[b,c]	3.43	0.82	0.53	1.45 (1.5)

[a] Device with HBL (TQB). [b] Device with HBL (TPBI). [c] The active layer was deposited from dichloromethane with 0.2% DIO.

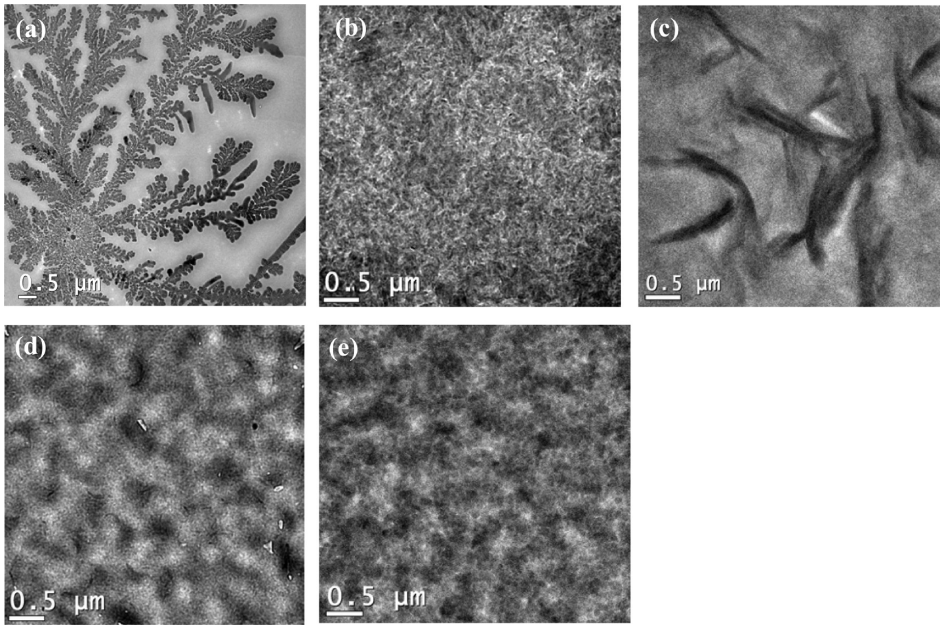

Figure 11. TEM images of blend thin films: (a) P3HT:NDI-2TH (1:2); (b) P3HT:NDI-3TH (1:3); (c) P3HT:NDI-4TH (1:4); (d) P3HT:NDI-2T (1:2); and (e) P3HT:NDI-3T (1:3).

dx.doi.org/10.1021/cm2019668 |*Chem. Mater.* 2011, 23, 4563–4577

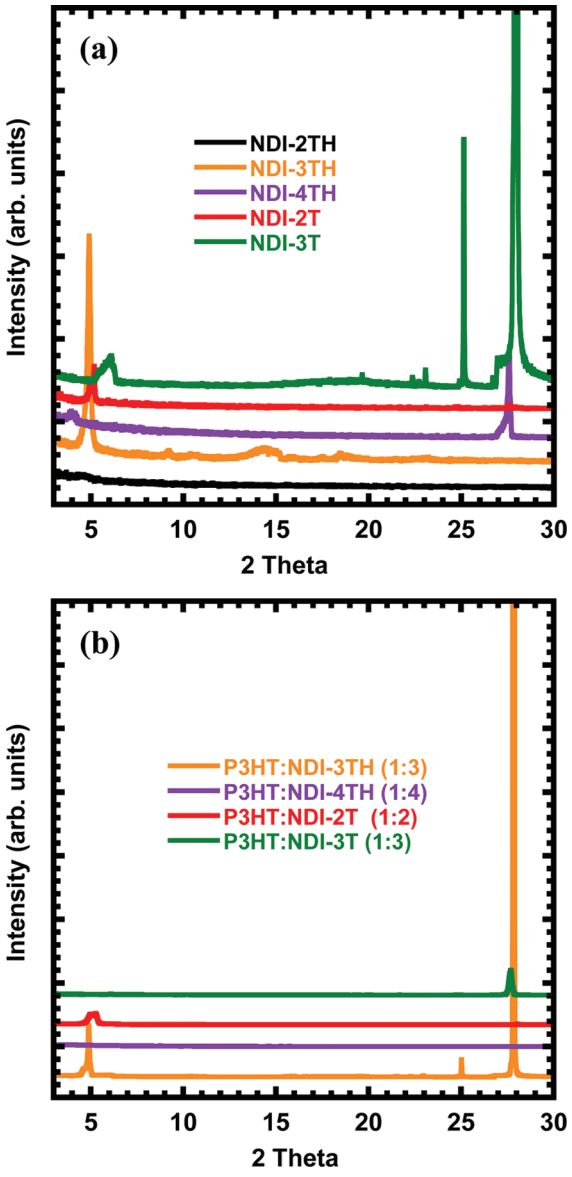

Figure 12. XRD patterns of (a) NDI acceptor materials and (b) P3HT:NDI-*n*TH or P3HT:*n*T blends.

Initial optimization of the P3HT:NDI-3TH devices was carried out to improve the power conversion efficiency, including the use of a processing additive, 1,8-diiodooctane (DIO), change of the solvent from chloroform to dichloromethane, incorporation of a P3HT layer (15 nm) as a buffer layer between the active layer and the anode, and insertion of a TPBI layer (3 nm) between the active layer and the cathode.[56] The resulting solar cells had a power conversion efficiency of 1.5% with an open circuit voltage of 0.82 V, an *FF* of 0.53, and a J_{sc} of 3.43 mA/cm^2 under 100 mW/cm^2 AM1.5 sunlight illumination. This efficiency is among the highest obtained to date in *non-fullerene* small-molecule based BHJ solar cells. The high efficiency obtained for the optimized device is due to a significant increase in the fill factor and short-circuit current density. The role of the processing additive is unclear thus far; however, further studies and device optimizations are underway. The incident photon-to-electron efficiency (IPCE), or external quantum efficiency spectrum, of the optimized P3HT:NDI-3TH (1:1) solar cell that gave 1.5% PCE is shown in Figure 10c. The photoresponse of this BHJ diode covers the entire visible region ranging 800−300 nm, with the highest IPCE of 15−16% at 470−600 nm. The J_{sc} calculated from IPCE is 3.00 mA/cm^2, which is 14% lower than that observed from $J-V$ measurement. Specific reasons for the discrepancy include degradation of the non-encapsulated solar cells when taken to a measurement facility in a different building, neglect of the J_{sc} contribution from the 300−350 nm wavelength region not covered by the IPCE spectrum, and spectral mismatch between the solar simulator and the solar spectrum. The IPCE spectrum clearly shows that both the NDI-3TH acceptor and P3HT donor contribute to light harvesting, exciton generation, and charge generation.

3.8. Morphology of BHJ Blend Films. The morphology of the BHJ P3HT:NDI-*n*TH and P3HT:NDI-*n*T blends, as revealed by TEM imaging, is shown in Figure 11. Three main types of morphology are observed: (i) a dendritic microstructure in which the acceptor material forms a dendritic phase or dendritic islands is seen in P3HT:NDI-2TH blend thin films (Figure 11a); (ii) a bicontinuous two-phase nanostructure is seen in blend thin films of P3HT:NDI-3TH (Figure 11b), P3HT:NDI-2T (Figure 11d), and P3HT:NDI-3T (Figure 11e); and (iii) a microstructure with micrometer scale crystallites of the acceptor material is seen in P3HT:NDI-4TH (Figure 11c). These morphologies are generally consistent with the observed performance of photovoltaic devices. The dendritic islands seen in NDI-2TH blends partly explain the absence of a photovoltaic response in the blends because photogenerated electrons in the electron-conducting phase all end up in dead paths and thus cannot be collected at the electrodes. Similarly, the lack of a photovoltaic response in P3HT:NDI-4TH can be partly understood from the rather small donor−acceptor area. In contrast, the bicontinuous nanoscale morphology of BHJ blends of P3HT:NDI-3TH and P3HT:NDI-*n*T (n = 2, 3) is consistent with the observed significant photovoltaic response of these blend systems. Furthermore, the smaller scale of P3HT and NDI-3TH domains in the morphology can explain the superior photovoltaic properties of this acceptor, compared to those of either NDI-2T or NDI-3T. Finally, the large variation in the morphology of these BHJ blend films is quite remarkable given the small variations in the molecular structure of the NDI acceptor materials. These morphological results suggest that there is a greater potential for tuning and even controlling the BHJ blend morphology in oligomer acceptors via synthesis than there is in fullerene acceptors.

To further investigate the solid state morphology, we performed XRD analysis on drop-casted films of the NDI acceptor materials and films of their blends with P3HT. Figure 12a presents the XRD patterns of films of the pure NDI-*n*TH and NDI-*n*T acceptor materials. NDI-2TH thin films showed no diffraction peaks before and after annealing, suggesting that this material does not readily crystallize. The X-ray diffraction pattern of NDI-3TH films showed a strong diffraction peak at $2\theta = 4.92°$, which corresponds to a *d*-spacing of 18.0 Å and can be assigned to (010) reflection. The diffraction pattern of NDI-4TH films showed a relatively weak diffraction peak at $2\theta = 3.98°$, which corresponds to a *d*-spacing of 22.17 Å and can be assigned to (100) reflection. A second strong diffraction peak in NDI-4TH thin films was also observed at $2\theta = 27.59°$, which corresponds to a *d*-spacing of 3.23 Å and can be assigned to the π-stacking direction. The X-ray diffraction pattern of NDI-2T films showed peaks at $2\theta = 5.19°$ and 27.6°, corresponding to *d*-spacings of

dx.doi.org/10.1021/cm2019668 |*Chem. Mater.* 2011, 23, 4563–4577

17.0 and 3.23 Å, respectively, whereas NDI-3T films showed diffraction peaks at 2θ = 6.2°, 19.6°, 22.3°, 22.9°, 25.1°, and 27.9°, corresponding to *d*-spacings of 14.2, 4.51, 3.98, 3.87, 3.54, and 3.2 Å, respectively. The strong diffraction peaks at 27.59° in NDI-4TH and 27.9° in NDI-3T films suggest that most of the molecular backbones oriented parallel, that is, *face-on* to the substrate. In contrast, the absence of the π-stacking peak in the XRD patterns of NDI-3TH and NDI-2T films suggests that the preferred molecular backbone orientation is perpendicular to the substrate.

The X-ray diffraction patterns of P3HT:NDI-*n*TH and P3HT:NDI-*n*T blend thin films are shown in Figure 12b. The X-ray diffraction pattern of P3HT:NDI-3TH blend films showed three diffraction peaks at 4.9, 25.0, and 27.8°, corresponding to *d*-spacings of 18.0, 3.55, and 3.2 Å. The strong new diffraction peak at 27.8° corresponds to the π-stacking, which suggests that most of NDI-3TH backbones are oriented parallel to the substrate. This *face-on* orientation is the preferred orientation for charge transport in photovoltaic devices. The XRD pattern of P3HT:NDI-4TH blend films showed no reflection peaks. This suggests that the blend of P3HT with NDI-4TH severely disturbs the molecular packing of NDI-4TH and gives an amorphous film. The diffraction pattern of P3HT:NDI-2T blend film (2θ = 5.26 and 27.9°) is very similar to the pure NDI-2T diffraction pattern, suggesting that there is no change in the molecular packing when a NDI-2T film is blended with P3HT. In contrast, the P3HT:NDI-3T blend film showed only one diffraction peak (2θ = 27.8°), compared to the five diffraction peaks observed in the pure NDI-3T film.

4. CONCLUSIONS

New oligomer semiconductors with donor−acceptor architecture based on oligothiophene donor and naphthalene diimide acceptor moieties, NDI-*n*TH and NDI-*n*T, have been synthesized and characterized. Single-crystal X-ray structures of NDI-3TH and NDI-4TH were obtained, revealing a slipped face-to-face π-stacking with relatively short intermolecular interactions (3.2−3.26 Å). The oligomer semiconductors had broad absorption bands with optical band gaps in the 1.4−2.1 eV range. The LUMO energy level of the series of oligomers was relatively constant at −4.0 to −4.1 eV, whereas the HOMO energy level could be tuned from −5.5 in NDI-3TH and NDI-4TH to −6.1 eV in NDI-1TH. Ambipolar field-effect charge transport was observed in all six materials with electron mobilities (μ_e) from 5.0×10^{-6} to 9.0×10^{-4} $cm^2/(V\ s)$ and hole mobilities (μ_h) from 2.2×10^{-5} to 2.1×10^{-3} $cm^2/(V\ s)$.

The homologous series of oligomer semiconductors, NDI-*n*TH (n = 1, 2, 3, 4) and NDI-*n*T (n = 2, 3), was used to evaluate factors essential to the design of *non-fullerene* acceptor materials for OPVs, including HOMO/LUMO energy levels offsets, optical absorption, band gap, charge transport, and phase-separated morphology of the BHJ active layer film. Solution-processed BHJ blends of each oligomer with P3HT showed a photovoltaic response when the oligomer charge transport was such that $\mu_e/\mu_h \geq 1$; oligomers having $\mu_e/\mu_h < 1$ did not show a photovoltaic response. Similarly, a photovoltaic response was not observed in P3HT:NDI-2TH, which showed a dendritic nanomorphology, and P3HT:NDI-4TH, which showed a microscale phase-separated morphology. P3HT:NDI-*n*T(H) blends showing a photovoltaic response had a bicontinuous nanoscale morphology, while light harvesting and exciton generation take place in both phases of the BHJ thin film. Bulk heterojunction devices with an active layer of P3HT:NDI-3TH (1:3) showed a power conversion efficiency of 1.5%, with an open circuit voltage of 820 mV, which is among the highest photovoltaic efficiencies obtained to date in *non-fullerene*, small molecule acceptor BHJ polymer solar cells. These results suggest that the identified set of criteria can provide a guide in the design of new acceptor materials for organic photovoltaics.

■ ASSOCIATED CONTENT

Supporting Information. Single crystal X-ray diffraction file (CIF), crystallographic table, TGA scans, DSC scans, cyclic voltammogram scans, optical microscope images, and solar cells data. This material is available free of charge via the Internet at http://pubs.acs.org.

■ AUTHOR INFORMATION

Corresponding Author
*E-mail: jenekhe@u.washington.edu.

■ ACKNOWLEDGMENT

This report is based on research (excitonic solar cells) supported by the U.S. DOE, Basic Energy Sciences, Division of Materials Science, under Award No. DE-FG02-07ER46467. The synthesis of the n-type oligomer semiconductors was supported by the NSF (DMR 0805259 and DMR 0120967) and, in part, by the ONR (N00014-11-1-0317), while the assembly and characterization of the nanowires were supported by the ONR (N00014-08-1-1148). E.A. received a UNCF/Merck Graduate Science Research Dissertation Fellowship. Part of this work was conducted at the University of Washington NanoTech User Facility, a member of the NSF National Nanotechnology Infrastructure Network (NNIN).

■ REFERENCES

(1) (a) Gunes, S.; Neugebauer, H.; Sariciftci, N. S. *Chem. Rev.* **2007**, *107*, 1324. (b) Thompson, B. C.; Fréchet, J. M. J. *Angew. Chem., Int. Ed.* **2008**, *47*, 58. (c) Coakley, K. M.; McGehee, M. D. *Chem. Mater.* **2004**, *16*, 4533. (d) Dennler, G.; Scharber, M. C.; Brabec, C. J. *Adv. Mater.* **2009**, *21*, 1323. (e) Chen, L.-M.; Hong, Z.; Li, G.; Yang, Y. *Adv. Mater.* **2009**, *21*, 1434.

(2) Gregg, B. A. *J. Phys. Chem. B* **2003**, *107*, 4688.

(3) (a) Ohkita, H.; Cook, S.; Astuti, Y.; Duffy, W.; Tierney, S.; Zhang, W.; Heeney, M.; McCulloch, I.; Nelson, J.; Bradly, D. D. C.; Durrant, J. R. *J. Am. Chem. Soc.* **2008**, *130*, 3030. (b) Clarke, T. M.; Durrant, J. R. *Chem. Rev.* **2010**, *110*, 6736. (c) Brédas, J.-L.; Norton, J. E.; Cornil, J.; Coropceanu, V. *Acc. Chem. Res.* **2009**, *42*, 1691. (d) Blom, P. W. M.; Mihailetchi, V. D.; Koster, L. J. A.; Markov, D. E. *Adv. Mater.* **2007**, *19*, 1551.

(4) (a) Antoniadis, A.; Hsieh, B. R.; Abkowitz, M. A.; Jenekhe, S. A.; Stolka, M. *Synth. Met.* **1994**, *62*, 265. (b) Marks, R. N.; Halls, J. J. M.; Bradley, D. D. C.; Friend, R. H.; Holmes, A. B. *J. Phys.: Condens. Matter* **1994**, *6*, 1379.

(5) (a) Tang, C. W. *Appl. Phys. Lett.* **1986**, *48*, 183. (b) Peumans, P.; Forrest, S. R. *Appl. Phys. Lett.* **2001**, *79*, 126. (c) Sariciftci, N. S.; Braun, D.; Zhang, C.; Srdanov, V. I.; Heeger, A. J.; Stucky, G.; Wudl, F. *Appl. Phys. Lett.* **1993**, *62*, 585.

(6) (a) Yu, G.; Heeger, A. J. *J. Appl. Phys.* **1995**, *78*, 4510. (b) Halls, J. J. M.; Walsh, C. A.; Greenham, N. C.; Marseglia, E. A.; Friend, R. H.; Moratti, S. C.; Holmes, A. B. *Nature* **1995**, *376*, 498.

(7) (a) Liang, Y.; Feng, D.; Wu, Y.; Tsai, S.-T.; Li, G.; Ray, C.; Yu, L. *J. Am. Chem. Soc.* **2009**, *131*, 7792. (b) Liang, Y.; Xu, Z.; Xia, J.; Tsai, S.-T.; Wu, Y.; Li, G.; Ray, C.; Yu, L. *Adv. Mater.* **2010**, *22*, E135. (c) Park, S. H.; Roy, A.; Beaupré, S.; Cho, S.; Coates, N.; Moon, J. S.; Moses, D.; Leclerc, M.; Lee, K.; Heeger, A. J. *Nat. Photonics* **2009**, *3*, 297. (d) Piliego, C.; Holcombe, T. W.; Douglas, J. D.; Woo, C. H.; Beaujuge, P. M.; Fréchet, J. M. J. *J. Am. Chem. Soc.* **2010**, *132*, 7595.

(8) (a) Ahmed, E.; Kim, F. S.; Xin, H.; Jenekhe, S. A. *Macromolecules* **2009**, *42*, 8615. (b) Xin, H.; Guo, X.; Kim, F. S.; Ren, G.; Watson, M. D.; Jenekhe, S. A. *J. Mater. Chem.* **2009**, *19*, 5303. (c) Bull, T. A.; Pingree, L. S. C.; Jenekhe, S. A.; Ginger, D. S.; Luscombe, C. K. *ACS Nano* **2009**, *3*, 627. (d) Wu, P.-T.; Xin, H.; Kim, F. S.; Ren, G.; Jenekhe, S. A. *Macromolecules* **2009**, *42*, 8817. (e) Guo, X.; Xin, H.; Kim, F. S.; Liyanage, A. D. T.; Jenekhe, S. A.; Watson, M. D. *Macromolecules* **2011**, *44*, 269. (f) Wu, P.-T.; Ren, G.; Jenekhe, S. A. *Macromolecules* **2010**, *43*, 3306–3313. (g) Subramaniyan, S.; Xin, H.; Kim, F. S.; Shoaee, S.; Durrant, J. R.; Jenekhe, S. A. *Adv. Energy Mater.* **2011**, *1*, 854−860.

(9) (a) Xin, H.; Kim, F. S.; Jenekhe, S. A. *J. Am. Chem. Soc.* **2008**, *130*, 5424. (b) Xin, H.; Ren, G.; Kim, F. S.; Jenekhe, S. A. *Chem. Mater.* **2008**, *20*, 6199.

(10) Walker, B.; Tamayo, A. B.; Dang, X.-D.; Zalar, P.; Seo, J. H.; Garcia, A.; Tantiwiwat, M.; Nguyen, T.-Q. *Adv. Funct. Mater.* **2009**, *19*, 3063.

(11) (a) Huynh, W. U.; Dittmer, J. J.; Alivisatos, A. P. *Science* **2002**, *295*, 2425. (b) Sun, B.; Marx, E.; Greenham, N. C. *Nano Lett.* **2003**, *3*, 961. (c) Liu, J.; Tanaka, T.; Sivula, K.; Alivisatos, A. P.; Fréchet, J. M. J. *J. Am. Chem. Soc.* **2004**, *126*, 6550. (d) Dayal, S.; Kopidakis, N.; Olson, D. C.; Ginley, D. S.; Rumbles, G. *Nano Lett.* **2010**, *10*, 239.

(12) Noone, K. M.; Strein, E.; Anderson, N. G.; Wu, P.-T.; Jenekhe, S. A.; Ginger, D. S. *Nano Lett.* **2010**, *10*, 2635.

(13) (a) Arango, A. C.; Carter, S. A.; Brock, P. J. *Appl. Phys. Lett.* **1999**, *74*, 1698. (b) Coakley, K. M.; McGehee, M. D. *Appl. Phys. Lett.* **2003**, *83*, 3380. (c) Kuo, C. Y.; Tang, W. C.; Gau, C.; Guo, T. F.; Jeng, D. Z. *Appl. Phys. Lett.* **2008**, *93*, 033307.

(14) (a) Kymakis, E.; Amaratunga, G. A. J. *Appl. Phys. Lett.* **2002**, *80*, 112. (b) Kymakis, E.; Alexandrou, I.; Amaratunga, G. A. J. *J. Appl. Phys.* **2003**, *93*, 1764. (c) Landi, B. J.; Raffaelle, R. P.; Castro, S. L.; Bailey, S. G. *Prog. Photovolt.: Res. Appl.* **2005**, *13*, 165. (d) Geng, J.; Zeng, T. *J. Am. Chem. Soc.* **2006**, *128*, 16827. (e) Ago, H.; Petritsch, K.; Shaffer, M. S. P.; Windle, A. H.; Friend, R. H. *Adv. Mater.* **1999**, *11*, 1281.

(15) (a) Liu, Z.; Liu, Q.; Huang, Y.; Ma, Y.; Yin, S.; Zhang, X.; Sun, W.; Chen, Y. *Adv. Mater.* **2008**, *20*, 3924. (b) Liu, Q.; Liu, Z.; Zhang, X.; Yang, L.; Zhang, N.; Pan, G.; Yin, S.; Chen, Y.; Wei, J. *Adv. Funct. Mater.* **2009**, *19*, 894.

(16) (a) Anthony, J. E. *Chem. Mater.* **2011**, *23*, 583. (b) Lloyd, M. T.; Anthony, J. E.; Malliaras, G. G. *Mater. Today* **2007**, *10*, 34.

(17) (a) Brunetti, F. G.; Gong, X.; Tong, M.; Heeger, A. J.; Wudl, F. *Angew. Chem., Int. Ed.* **2010**, *49*, 532. (b) Sonar, P.; Ng, G.-M.; Lin, T. T.; Dodabalapur, A.; Chen, Z.-K. *J. Mater. Chem.* **2010**, *20*, 3626. (c) Karsten, B. P.; Bijleveld, J. C.; Janssen, R. A. J. *Macromol. Rapid Commun.* **2010**, *31*, 1554.

(18) (a) Dittmer, J. J.; Marseglia, E. A.; Friend, R. H. *Adv. Mater.* **2000**, *12*, 1270. (b) Schmidt-Mende, L.; Fechtenkötter, A.; Müllen, K.; Moons, E.; Friend, R. H.; MacKenzie, J. D. *Science* **2001**, *293*, 1119. (c) Li, J.; Dierschke, F.; Wu, J.; Grimsdale, A. C.; Müllen, K. *J. Mater. Chem.* **2006**, *16*, 96. (d) Rajaram, S.; Armstrong, P. B.; Kim, B. J.; Fréchet, J. M. J. *Chem. Mater.* **2009**, *21*, 1775.

(19) (a) de Bettignies, R.; Nicolas, Y.; Blanchard, P.; Levillain, E.; Nunzi, J.-M.; Roncali, J. *Adv. Mater.* **2003**, *15*, 1939. (b) Shin, W. S.; Jeong, H.-H.; Kim, M.-K.; Jin, S.-H.; Kim, M.-R.; Lee, J.-K.; Lee, J.-W.; Gal, Y.-S. *J. Mater. Chem.* **2006**, *16*, 384. (c) Bu, L.; Guo, X.; Yu, B.; Qu, Y.; Xie, Z.; Yan, D.; Geng, Y.; Wang, F. *J. Am. Chem. Soc.* **2009**, *13*, 13242. (d) Sharma, G. D.; Suresh, P.; Mikroyannidis, J. A.; Stylianakis, M. M. *J. Mater. Chem.* **2010**, *20*, 561.

(20) (a) Shin, R. Y. C.; Kietzke, T.; Sudhakar, S.; Dodabalapur, A.; Chen, Z.-K.; Sellinger, A. *Chem. Mater.* **2007**, *19*, 1892. (b) Inal, S.; Castellani, M.; Sellinger, A.; Neher, D. *Macromol. Rapid Commun.* **2009**, *30*, 1263. (c) Woo, C. H.; Holcombe, T. W.; Unruh, D. A.; Sellinger, A.; Fréchet, J. M. J. *Chem. Mater.* **2010**, *22*, 1673.

(21) (a) Lim, Y. F.; Shu, Y.; Parkin, S. R.; Anthony, J. E.; Malliaras, G. G. *J. Mater. Chem.* **2009**, *19*, 3049. (b) Shu, Y.; Lim, Y.-F.; Li, Z.; Purushothaman, B.; Hallani, R.; Kim, J. E.; Parkin, S. R.; Malliaras, G. G.; Anthony, J. E. *Chem. Sci.* **2011**, *2*, 363.

(22) Sonar, P.; Lim, J. P. F.; Chan, K. L. *Energy Environ. Sci.* **2011**, *4*, 1558.

(23) (a) Alam, M. M.; Jenekhe, S. A. *Chem. Mater.* **2004**, *16*, 4647. (b) Jenekhe, S. A.; Yi, S. *Appl. Phys. Lett.* **2000**, *77*, 2635.

(24) (a) Kietzke, T.; Höerhold, H.-H.; Neher, D. *Chem. Mater.* **2005**, *17*, 6532. (b) Koetse, M. M.; Sweelssen, J.; Hoekerd, K. T.; Schoo, H. F. M.; Veenstra, S. C.; Kroon, J. M.; Yang, X.; Loos, J. *Appl. Phys. Lett.* **2006**, *88*, 083504. (c) Holcombe, T. W.; Woo, C. H.; Kavulak, D. F. J.; Thompson, B. C.; Fréchet, J. M. J. *J. Am. Chem. Soc.* **2009**, *131*, 14160.

(25) (a) Zhan, X.; Tan, Z.; Domercq, B.; An, Z.; Zhang, X.; Barlow, S.; Li, Y.; Zhu, D.; Kippelen, B.; Marder, S. R. *J. Am. Chem. Soc.* **2007**, *129*, 7246. (b) Zhou, E.; Cong, J.; Wei, Q.; Tajima, K.; Yang, C.; Hashimoto, K. *Angew. Chem., Int. Ed.* **2011**, *50*, 2799. (c) Zhang, Q.; Cirpan, A.; Russell, T. P.; Emrick, T. *Macromolecules* **2009**, *42*, 1079.

(26) (a) McNeill, C. R.; Abrusci, A.; Zaumseil, J.; Wilson, R.; McKiernan, M. J.; Burroughes, J. H.; Halls, J. J. M.; Greenham, N. C.; Friend, R. H. *Appl. Phys. Lett.* **2007**, *90*, 193506. (b) McNeill, C. R.; Halls, J. J. M.; Wilson, R.; Whiting, G. L.; Berkebile, S.; Ramsey, M. G.; Friend, R. H.; Greenham, N. C. *Adv. Funct. Mater.* **2008**, *18*, 2309.

(27) (a) Allemand, P.-M.; Koch, A.; Wudl, F.; Rubin, Y.; Diederich, F.; Alvarez, M. M.; Anz, S. J.; Whetten, R. J. *J. Am. Chem. Soc.* **1991**, *113*, 1050. (b) Yu, G.; Gao, J.; Hummelen, J. C.; Wudl, F.; Heeger, A. J. *Science* **1995**, *270*, 1789.

(28) (a) Singh, T. B.; Marjanović, N.; Matt, G. J.; Günes, S.; Sarciftci, N. S.; Ramil, A. M.; Andreev, A.; Sitter, H.; Schwödiauer, R.; Bauer, S. *Org. Electron.* **2005**, *6*, 105. (b) Itaka, K.; Yamashiro, M.; Yamaguchi, J.; Haemori, M.; Yaginuma, S.; Matsumoto, Y.; Kondo, M.; Koinuma, H. *Adv. Mater.* **2006**, *18*, 1713. (c) Anthopoulos, T. D.; Singh, B.; Marjanović, N.; Sariciftci, N. S.; Ramil, A. M.; Sitter, H.; Cölle, M.; de Leeuw, D. M. *Appl. Phys. Lett.* **2006**, *89*, 213504. (d) Zhang, X.-H.; Domercq, B.; Kippelen, B. *Appl. Phys. Lett.* **2007**, *91*, 092114.

(29) (a) Xin, H.; Reid, O. G.; Ren, G.; Kim, F. S.; Ginger, D. S.; Jenekhe, S. A. *ACS Nano* **2010**, *4*, 1861. (b) Ren, G.; Wu, P.-T.; Jenekhe, S. A. *ACS Nano* **2011**, *5*, 376. (c) Ren, G.; Wu, P.-T.; Jenekhe, S. A. *Chem. Mater.* **2010**, *22*, 2020. (d) Wu, P.-T.; Ren, G.; Li, C.; Mezzenga, R.; Jenekhe, S. A. *Macromolecules* **2009**, *42*, 2317–2320.

(30) Kim, F. S.; Ren, G.; Jenekhe, S. A. *Chem. Mater.* **2011**, *23*, 682.

(31) (a) Lee, J. K.; Ma, W. L.; Brabec, C. J.; Yuen, J.; Moon, J. S.; Kim, J. Y.; Lee, K.; Bazan, G. C.; Heeger, A. J. *J. Am. Chem. Soc.* **2008**, *130*, 3619. (b) Peet, J.; Kim, J. Y.; Coates, N. E.; Ma, W. L.; Moses, D.; Heeger, A. J.; Bazan, G. C. *Nat. Mater.* **2007**, *6*, 497.

(32) (a) Yang, X.; Loos, J. *Macromolecules* **2007**, *40*, 1353. (b) Yang, X.; Loos, J.; Veenstra, S. C.; Verhees, W. J. H.; Wienk, M. M.; Kroon, J. M.; Michels, M. A. J.; Janssen, R. A. J. *Nano Lett.* **2005**, *5*, 579. (c) Yao, Y.; Hou, J.; Xu, Z.; Li, G.; Yang, Y. *Adv. Funct. Mater.* **2008**, *18*, 1783. (d) Berson, S.; De Bettignies, R.; Bailly, S.; Guillerez, S. *Adv. Funct. Mater.* **2007**, *17*, 1377.

(33) (a) Brabec, C. J.; Cravino, A.; Meissner, D.; Sariciftci, N. S.; Fromherz, T.; Rispens, M. T.; Sanchez, L.; Hummelen, J. C. *Adv. Funct. Mater.* **2001**, *11*, 374. (b) Gadisa, A.; Svensseon, M.; Andersson, M. R.; Inganäs, O. *Appl. Phys. Lett.* **2004**, *84*, 1609. (c) Potscavage, W. J.; Sharma, A.; Kippelen, B. *Acc. Chem. Res.* **2009**, *42*, 1758. (d) Perez, M. D.; Borek, C.; Forrest, S. R.; Thompson, M. E. *J. Am. Chem. Soc.* **2009**, *131*, 9281. (e) Vandewal, K.; Tvingstedt, K.; Gadisa, A.; Inganäs, O.; Manca, J. V. *Nat. Mater.* **2009**, *8*, 904.

(34) Wienk, M. M.; Kroon, J. M.; Verhees, W. J. H.; Knol, J.; Hummelen, J. C.; Hal, P. A. V.; Janssen, R. A. J. *Angew. Chem., Int. Ed.* **2003**, *42*, 3371.

(35) (a) Reese, M. O.; Nardes, A. M.; Rupert, B. L.; Larsen, R. E.; Olson, D. C.; Lloyd, M. T.; Shaheen, S. E.; Ginley, D. S.; Rumbles, G.; Kopidakis, N. *Adv. Funct. Mater.* **2010**, *20*, 3476. (b) Hummelen, J. C.; Knol, J.; Sanchez, L. Organic photovoltaics. In *Proceedings of SPIE*;

Kafafi, Z. H., Ed.; SPIE: 2001; Vol. *4108*, p 76. (c) Creegan, K. M.; Robbins, J. L.; Robbins, J. L.; Millar, J. M.; Sherwood, R. D.; Tindall, P. J.; Cox, D. M.; Smith, A. B.; McCauley, J. P.; Jones, D. R.; Gallagher, R. T. *J. Am. Chem. Soc.* **1992**, *114*, 1103.

(36) (a) Wudl, F. *Acc. Chem. Res.* **1992**, *25*, 157. (b) Hummelen, J. C.; Knight, B. W.; LePeq, F.; Wudl, F.; Yao, J.; Wilkins, C. L. *J. Org. Chem.* **1995**, *60*, 532.

(37) (a) Brabec, C. J.; Winder, C.; Sariciftci, N. S.; Hummelen, J. C.; Dhanabalan, A.; Hal, P. A. V.; Janssen, R. A. J. *Adv. Funct. Mater.* **2002**, *12*, 709. (b) Winder, C.; Matt, G.; Hummelen, J. C.; Janssen, R. A. J.; Sariciftci, N. S.; Brabec, C. J. *Thin Solid Films* **2002**, *403*, 373. (c) Gong, X.; Tong, M.; Brunetti, F. G.; Seo, J.; Sun, Y.; Moses, D.; Wudl, F.; Heeger, A. J. *Adv. Mater.* **2011**, *23*, 2272.

(38) (a) Zhao, W.; Kahn, A. *J. Appl. Phys.* **2009**, *105*, 123711. (b) Guan, Z.-L.; Kim, J. B.; Wang, H.; Jaye, C.; Fischer, D. A.; Loo, Y.-L.; Kahn, A. *Org. Electron.* **2010**, *11*, 1779. (c) Akaike, K.; Kanai, K.; Yoshida, H.; Tsutsumi, J.; Nishi, T.; Sato, N.; Ouchi, Y.; Seki, K. *J. Appl. Phys.* **2008**, *104*, 023710.

(39) (a) Jenekhe, S. A.; Lu, L.; Alam, M. M. *Macromolecules* **2001**, *34*, 7315. (b) Zhu, Y.; Champion, R. D.; Jenekhe, S. A. *Macromolecules* **2006**, *39*, 8712. (c) Champion, R. D.; Cheng, K.-F.; Pai, C.-L.; Chen, W.-C.; Jenekhe, S. A. *Macromol. Rapid Commun.* **2005**, *26*, 1835.

(40) (a) Katz, H. E.; Lovinger, A. J.; Johnson, J.; Kloc, C.; Siegrist, T.; Li, W.; Lin, Y.-Y.; Dodabalapur, A. *Nature* **2000**, *404*, 478. (b) Jung, B. J.; Lee, K.; Sun, J.; Andreou, A. G.; Katz, H. E. *Adv. Funct. Mater.* **2010**, *20*, 2930.

(41) (a) Jones, B. A.; Facchetti, A.; Marks, T. J.; Wasielewski, M. R. *Chem. Mater.* **2007**, *19*, 2703. (b) Polander, L. E.; Tiwari, S. P.; Pandey, L.; Seifried, B. M.; Zhang, Q.; Barlow, S.; Risko, C.; Brédas, J.-L.; Kippelen, B.; Marder, S. R. *Chem. Mater.* **2011**, *23*, 3408.

(42) (a) See, K. C.; Landis, C.; Sarjeant, A.; Katz, H. E. *Chem. Mater.* **2008**, *20*, 3609. (b) Gawrys, P.; Boudinet, D.; Kornet, A.; Djurado, D.; Pouget, S.; Verilhac, J.-M.; Zagorska, M.; Pron, A. *J. Mater. Chem.* **2010**, *20*, 1913.

(43) (a) Yan, H.; Chen, Z.; Zheng, Y.; Newman, C.; Quinn, J. R.; Dötz, F.; Kastler, M.; Facchetti, A. *Nature* **2009**, *457*, 679. (b) Durban, M. M.; Kazarinoff, P. D.; Luscombe, C. K. *Macromolecules* **2010**, *43*, 6348.

(44) Kim, F. S.; Guo, X.; Watson, M. D.; Jenekhe, S. A. *Adv. Mater.* **2010**, *22*, 478.

(45) Guo, X.; Watson, M. D. *Org. Lett.* **2008**, *10*, 5333.

(46) (a) Salhi, F.; Lee, B.; Metz, C.; Bottomley, L. A.; Collard, D. M. *Org. Lett.* **2002**, *4*, 3195. (b) Bair, J. S.; Harrison, R. G. *J. Org. Chem.* **2007**, *72*, 6653.

(47) (a) Facchetti, A.; Yoon, M.-H.; Stern, C. L.; Hutchison, G. R.; Ratner, M. A.; Marks, T. J. *J. Am. Chem. Soc.* **2004**, *126*, 13480. (b) Garnier, F.; Hajlaoui, R.; Kassmi, A. E.; Horowitz, G.; Laigre, L.; Porzio, W.; Armanini, M.; Provasoli, F. *Chem. Mater.* **1998**, *10*, 3334. (c) Garnier, F.; Yasser, A.; Hajlaoui, R.; Horowitz, G.; Deloffre, F.; Servet, B.; Ries, S.; Alnot, P. *J. Am. Chem. Soc.* **1993**, *115*, 8716. (d) Kleiner-Shuler, L.; Brittain, R.; Johnston, M. R.; Hipps, K. W. *J. Phys. Chem. C* **2008**, *112*, 14907.

(48) (a) Zhao, Y. S.; Fu, H.; Peng, A.; Ma, Y.; Liao, Q.; Yao, J. *Acc. Chem. Res.* **2010**, *43*, 409. (b) Geng, J.; Zhou, W.; Skelton, P.; Yue, W.; Kinloch, I. A.; Windle, A. H.; Johnson, B. F. G. *J. Am. Chem. Soc.* **2008**, *130*, 2527. (c) Lee, D.-C.; Jang, K.; McGrath, K. K.; Uy, R.; Robins, K. A.; Hatchett, D. W. *Chem. Mater.* **2008**, *20*, 3688. (d) Lee, D.-C.; McGrath, K. K.; Jang, K. *Chem. Commun.* **2008**, 3636. (e) Ahmed, E.; Earmme, T.; Ren, G.; Jenekhe, S. A. *Chem. Mater.* **2010**, *22*, 5786.

(49) (a) Schenning, A. P. H. J.; Meijer, E. W. *Chem. Commun.* **2005**, 3245. (b) Würthner, F. *Chem. Commun.* **2004**, *14*, 1564. (c) Oh, J. H.; Lee, H. W.; Mannsfeld, S.; Stoltenberg, R. M.; Jung, E.; Jin, Y. W.; Kim, J. M.; Yoo, J.-B.; Bao, Z. *Proc. Natl. Acad. Sci. U.S.A.* **2009**, *106*, 6065. (d) Briseno, A. L.; Mannsfeld, S. C. B.; Reese, C.; Hancock, J. M.; Xiong, Y.; Jenekhe, S. A.; Bao, Z.; Xia, Y. *Nano Lett.* **2007**, *7*, 2847. (e) Che, Y.; Datar, A.; Balakrishnan, K.; Zang, L. *J. Am. Chem. Soc.* **2007**, *129*, 7234–7235. (f) Balakrishnan, K.; Datar, A.; Oitker, R.; Chen, H.; Zuo, J.; Zang, L. *J. Am. Chem. Soc.* **2005**, *127*, 10496–10497.

(50) (a) Kulkarni, A. P.; Tonzola, C. J.; Babel, A.; Jenekhe, S. A. *Chem. Mater.* **2004**, *16*, 4556. (b) Agrawal, A. K.; Jenekhe, S. A. *Chem. Mater.* **1996**, *8*, 579.

(51) (a) Hancock, J. M.; Gifford, A. P.; Champion, R. D.; Jenekhe, S. A. *Macromolecules* **2008**, *41*, 3588. (b) Zhu, Y.; Kulkarni, A. P.; Wu, P.-T.; Jenekhe, S. A. *Chem. Mater.* **2008**, *20*, 4200.

(52) (a) Pope, M.; Swenberg, C. E. *Electronic Process in Organic Crystals and Polymers*, 2nd ed.; Oxford University Press: New York, 1999. (b) Arkhipov, V. I.; Bassler, H. *Phys. Status Solidi A* **2004**, *201*, 1152.

(53) (a) Zaumseil, J.; Sirringhaus, H. *Chem. Rev.* **2007**, *107*, 1296. (b) Babel, A.; Jenekhe, S. A. *Adv. Funct. Mater.* **2004**, *14*, 891.

(54) Earmme, T.; Ahmed, E.; Jenekhe, S. A. *Adv. Mater.* **2010**, *22*, 4744.

(55) Chirvase, D.; Parisi, J.; Hummelen, J. C.; Dyakonov, V. *Nanotechnology* **2004**, *15*, 1317.

(56) Ren, G.; Ahmed, E.; Jenekhe, S. A. *Adv. Energy Mater.* **2011**, *1*, 946−953.